1

Charged Leptons

Conveners: B. C. K. Casey, Y. Grossman, D. G. Hitlin

J. Albrecht, M. Artuso, R. H. Bernstein, D. N. Brown, B. C. K. Casey, C.-h. Cheng, V. Cirigliano, A. Cohen, F. Grancagnolo, A. Deshpande, B. Echenard, D. Glenzinski, M. Gonzalez-Alonso Y. Grossman, R. Harnik, D. G. Hitlin, B. Kiburg, G. Lim, Z.-T. Lu, D. McKeen, J. P. Miller, M. Ramsey-Musolf, R. Ray, M. Rominsky, P. Winter

Contents

1.1 Overview

The theme of the "Snowmass on the Mississippi" exercise can be simply summed up as "How do we find New Physics?". The Intensity Frontier answer evokes the power and reach of virtual processes in both finding evidence for New Physics and constraining its properties. Experiments in the lepton sector of the Intensity Frontier, by searching for rare decay processes involving lepton flavor violation and *CP*-violation, and by making precision measurements of quantities whose value is extremely well-predicted in the Standard Model, can advance our understanding of the most basic features of the Standard Model for which we currently have no rationale. Why are there three lepton families? Since lepton flavor conservation is violated in the neutrino sector, is it violated in the charged lepton sector as well? Why are the patterns of lepton and quark flavor mixing so different?

Charged leptons are unique in several ways:

- They directly probe the couplings of new particles to leptons. This is unique in that the current energy frontier machine, the CERN LHC, is a hadron collider. It is very effective at probing the quark sector, but is significantly more limited in the lepton sector.
- Very precise measurements and sensitive searches can be made at a level that is difficult to achieve in other sectors.
- They can be studied using a diverse set of independent processes. The combination of these studies can provide additional insights into the structure of the lepton sector.
- Hadronic uncertainties in the Standard Model predictions are either insignificant, or in the case of muon $g-2$, are controlled using independent data sets.
- There are many cases, in particular charged lepton flavor violation (CLFV), where any signal would be an indisputable discovery of New Physics.

There are important charged lepton observables that are best studied using electrons, most notably the electron electric dipole moment (EDM). In most cases, these experiments are performed using outer-shell or shared electrons in either atoms or molecules. These topics are covered in detail by the Nucleons/Nuclei/Atoms working group; we refer the reader to the that chapter of this document.

The program of studies of charged leptons is diverse, encompassing highly optimized, single-purpose experiments that focus on near-forbidden interactions of muons and multi-purpose experiments that take advantage of the large τ-pair production cross section at B or τ/charm factories . Very large improvements in sensitivity are possible in the near future; even larger sensitivity gains can be made at Project X. New experiments such as Mu2e can probe rare processes at rates five orders of magnitude more sensitive than current bounds. At this level of sensitivity many models predict that there will be observations of SM-forbidden processes, not just limits. These improvements will be a significant part of the program to understand new short-distance dynamics or new ultra-weak interactions.

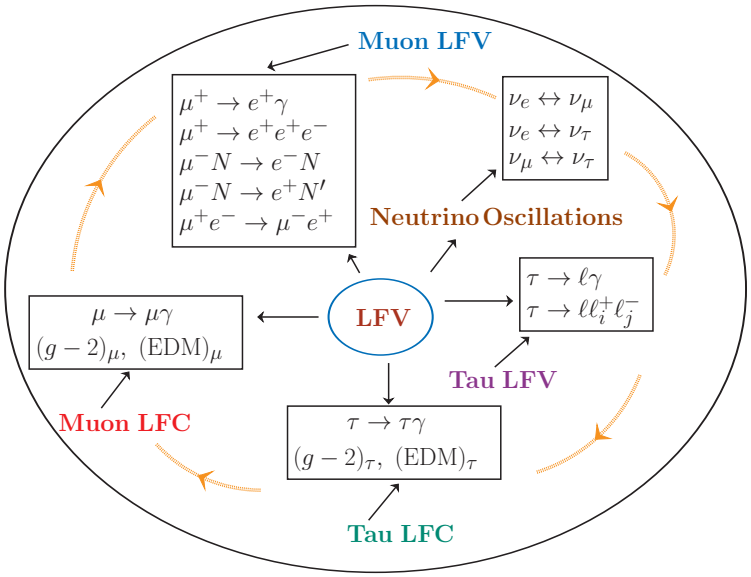

Figure 1-1. *Interconnection between various lepton flavor violating and lepton flavor conserving processes.*

Aside from being an intergral part of the broader Intensity Frontier program, studies of the charged lepton sector provide a vital link to the Energy Frontier. In the same way that, taken together, the results of individual charged lepton experiment are more sensitive to New Physics, charged lepton sector results as a whole are more powerful considered in concert with other Intensity and Energy Frontier experiments. In particular, there are three domains in which such combined results are a crucial probe of New Physics. First, since neutrinos and charged leptons form a natural doublet, one would expect any New Physics effects in neutrinos to also be seen in sufficiently sensitive charged lepton experiments. Second, any complete theory of flavor generation and the observed matter-antimatter asymmetry of the universe must relate flavor and *CP* (or T) violation in the heavy quark, neutrino, and charged lepton sectors. Third, any theory that predicts new particles or interactions at the LHC must also account for the virtual effects of those particles on decays and interactions of charged leptons and heavy quarks. Thus, the major expansion in the study of charged leptons now underway is a natural extension of the successful heavy quark, neutrino and energy frontier programs of the previous decades.

A fourth domain is the probe of new ultra-weak, low energy interactions, referred to collectively as hidden or dark sectors. Here, charged lepton experiments overlap with a wide variety of experiments at the Intensity, Cosmic, and Energy fFrontiers. A large experimental program is now under way to directly probe for new hidden sectors, particularly in regions of parameter space consistent with the muon $g-2$ anomaly. This program is covered in detail in the "New Light Weakly-Coupled Particles" chapter of this report.

Fig. 1-1 schematically depicts the interconnection between various flavor-conserving and -violating processes in the lepton sector. In an underlying theory, neutrino flavor oscillations, charged lepton flavor violation, the anomalous magnetic moments, and permanent electric dipole moments are all related. Each experimental avenue we pursue allows us to uncover further attributes of the underlying theory.

There are many important physical observables potentially sensitive to New Physics effects in charged lepton processes. Below, they are split into flavor violating observables and flavor conserving observables such as $g-2$, EDMs, and parity violation measurements. Tau decays offer a unique opportunity to simultaneously

study flavor-conserving, flavor-violating, *CP*-violating, and *T*-violating effects and are discussed in their own section below.

1.2 Flavor-Violating Processes

1.2.1 Theory Overview

Neutrino flavor oscillations are well established. This requires charged lepton flavor violation at some level as well. However flavor violation in charged lepton interactions has never been observed. If neutrino mass is the only source of new physics, and if the mass generation occurs at a very high energy scale, CLFV processes are highly suppressed. For example, if neutrinos are Dirac particles, the branching ratio for $\mu \to e\gamma$ is

$$BR(\mu \to e\gamma) = \frac{3\alpha}{32\pi}\left|\sum_i U^*_{\mu i}U_{ei}\frac{m^2_{\nu_i}}{m^2_W}\right|^2 \sim 10^{-52} \tag{1.1}$$

where U_{ei} are the leptonic mixing matrix elements. This value, which suffers from extreme suppression from the small neutrino masses, is experimentally inaccessible. In many extensions of the Standard Model however, there are much larger contributions to CLFV and current experimental bounds set strict limits on the parameter space available for new physics models.

The effective Lagrangian relevant for the $\mu \to e\gamma$ and $\mu^+ \to e^+e^-e^+$ decays can be parametrized, regardless of the origin of CLFV, as

$$\begin{aligned}\mathcal{L}_{\mu\to e\gamma,eee} = &-\frac{4G_F}{\sqrt{2}}\left[m_\mu A_R \overline{\mu_R}\sigma^{\mu\nu}e_L F_{\mu\nu} + m_\mu A_L \overline{\mu_L}\sigma^{\mu\nu}e_R F_{\mu\nu}\right.\\ &+g_1(\overline{\mu_R}e_L)(\overline{e_R}e_L) + g_2(\overline{\mu_L}e_R)(\overline{e_L}e_R)\\ &+g_3(\overline{\mu_R}\gamma^\mu e_R)(\overline{e_R}\gamma_\mu e_R) + g_4(\overline{\mu_L}\gamma^\mu e_L)(\overline{e_L}\gamma_\mu e_L)\\ &\left.+g_5(\overline{\mu_R}\gamma^\mu e_R)(\overline{e_L}\gamma_\mu e_L) + g_6(\overline{\mu_L}\gamma^\mu e_L)(\overline{e_R}\gamma_\mu e_R) + h.c.\right].\end{aligned} \tag{1.2}$$

The decay $\mu \to e\gamma$ is mediated by the first two terms of Eq. (1.2), the dipole terms. These terms, as well as the remaining contact terms, all contribute to the decay $\mu^+ \to e^+e^-e^+$. The relative strength of these decay rates depends on the relative strength of the dipole and contact terms. Turning this around, searches for these two decays reveal much about the underlying flavor structure. In some models the dipole contribution dominates both decays. In this case, a simple relation exists for the relative branching ratio:

$$\frac{B(\mu^+ \to e^+e^-e^+)}{B(\mu^+ \to e^+\gamma)} \simeq \frac{\alpha}{3\pi}\left(\ln(\frac{m^2_\mu}{m^2_e}) - \frac{11}{4}\right) = 0.006. \tag{1.3}$$

However, contact terms arise frequently in popular models where the relation Eq. (1.3) does not hold. A good example is the type II seesaw mechanism for small neutrino masses. Here, one does not add right-handed neutrinos to the spectrum, rather one includes an iso–triplet scalar $\Delta = (\Delta^{++}, \Delta^+, \Delta^0)$ with quantum numbers $(1, 3, +2)$ under $SU(3)_c \times SU(2)_L \times U(1)_Y$. Neutrino masses are generated via the Yukawa coupling $\frac{f_{ij}}{2}\ell_i^T C\ell_j\Delta$, once a nonzero $\langle\Delta^0\rangle$ develops. The doubly charged scalar Δ^{++} could mediate the decay $\mu^+ \to e^+e^-e^+$ at tree level. In this case, the branching ratios for $\mu \to e\gamma$ and $\mu^+ \to e^+e^-e^+$ become comparable.

Equally important as the decays $\mu \to e\gamma$ and $\mu^+ \to e^+e^-e^+$ is the coherent $\mu^-N \to e^-N$ conversion process in nuclei. Muonic atoms are formed when negative muons are stopped in matter. In the ground state of

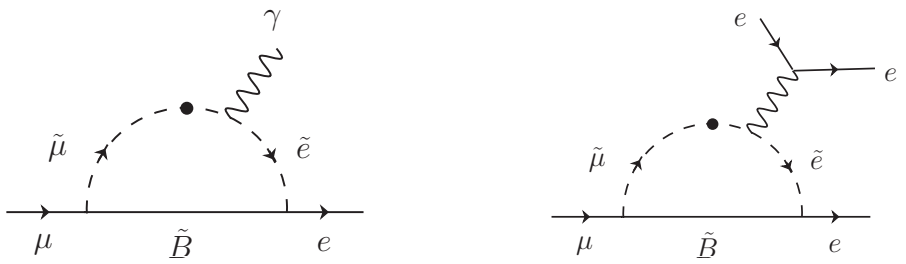

Figure 1-2. *$\mu \to e\gamma$ decay mediated by SUSY particles (left panel), and $\mu \to 3e$ decay (right panel).*

these atoms, the muon can decay in orbit or be captured with the emission of a neutrino via the process $\mu^- + (A, Z) \to \nu_\mu + (A, Z-1)$. If there are new sources of CLFV, muon capture without the emission of a neutrino can occur: $\mu^- + (A, Z) \to e^- + (A, Z)$. This would occur in supersymmetry (SUSY) via the diagram of Fig. 1-2, when the photon is attached to a quark line. Like $\mu^+ \to e^+e^-e^+$, this process can occur through dipole interactions or through contact interactions. Such contact interactions arise naturally in leptoquark models at the tree level, while in SUSY the dipole interactions dominate. If only the dipole couplings are important, one can obtain a relation for the ratio of rates

$$\frac{B(\mu^+ \to e^+\gamma)}{B(\mu^- N \to e^- N)} = \frac{96\pi^3\alpha}{G_F^2 m_\mu^4} \cdot \frac{1}{3 \cdot 10^{12} B(A,Z)} \simeq \frac{428}{B(A,Z)}, \tag{1.4}$$

where $B(A, Z)$ is a function of the atomic number and atomic weight, with its value ranging from 1.1 to 2.2 for Al, Ti and Pb atoms. The best limits on these processes are $B(\mu^- + \mathrm{Ti} \to e^- + \mathrm{Ti}) < 4.3 \times 10^{-12}$ [**?**] and $B(\mu^- + \mathrm{Au} \to e^- + \mathrm{Au}) < 7.0 \times 10^{-13}$ [3] from experiments conducted at PSI. For these searches the limits quoted are with respect to the muon capture process $\mu^- + (A, Z) \to \nu_\mu + (A, Z-1)$. Future experiments can improve tremendously on these limits down to 10^{-18}.

A related process is the incoherent, lepton number violating process $\mu^- + (A, Z) \to e^+ + (A, Z-2)^*$, which occurs in left–right symmetric models via the exchange of right–handed neutrinos and $W_R^\pm$ gauge bosons. The best limit presently on this process is $B(\mu^- + \mathrm{Ti} \to e^+ + \mathrm{Ca}) < 1.7 \times 10^{-12}$, also from PSI. TeV scale left–right symmetry predicts observable rates for this transition.

CLFV could also be seen in other muonic systems. Muonium is a (μ^+e^-) bound state analogous to the hydrogen atom, which in the presence of a CLFV interaction can oscillate into antimuonium (μ^-e^+). The doubly charged scalar of the seesaw model, the left–right symmetric model, or the radiative neutrino mass model would all lead to this process. If the Lagrangian for this process is parametrized as

$$H_{\mathrm{Mu}\overline{\mathrm{Mu}}} = \left(\frac{G_{\mathrm{Mu}\overline{\mathrm{Mu}}}}{\sqrt{2}}\right) \overline{\mu}\gamma_\lambda(1-\gamma_5)e\overline{\mu}\gamma^\lambda(1-\gamma_5)e + h.c., \tag{1.5}$$

the current limit from PSI experiments is $G_{\mathrm{Mu}\overline{\mathrm{Mu}}} < 0.003\, G_F$, with room for improvement by several orders of magnitude in the near future.

1.2.1.1 CLFV Decays in Specific New Physics Models

If we assume that neutrino mass is generated by a seesaw mechanism [**?**], we can see effects in CLFV if the seesaw scale is low [**?**]. It is perhaps more natural that the seesaw mechanism is realized at a very high energy scale, $M_R \sim 10^{10} - 10^{14}$ GeV. In this case there can be significant CLFV provided that there is some

new physics at the TeV scale. Below we briefly mention two such scenarios, SUSY and Randall-Sundrum warped extra dimensions (RS).

Implementing the seesaw mechanism within the context of SUSY leads to a new source of CLFV. In a momentum range between M_R and $M_{\rm Pl}$, where $M_{\rm Pl}$ is the fundamental Planck scale, the right-handed neutrinos are active and their Dirac Yukawa couplings with the lepton doublets induce flavor violation among the sleptons. The sleptons must have masses of order TeV or less, if SUSY is to solve the hierarchy problem, and they carry information on flavor violation originating from the seesaw. Specifically, the squared masses of the sleptons would receive flavor violating contributions given by

$$(m^2_{\tilde{l}_L})_{ij} \simeq -\frac{1}{8\pi^2}(Y_\nu^\dagger Y_\nu)_{ij}(3m_0^2 + |A_0|^2)\ln\left(\frac{M_{\rm Pl}}{M_R}\right) \tag{1.6}$$

where Y_ν is the Dirac Yukawa coupling of the neutrinos, and m_0 and A_0 are SUSY breaking mass parameters of order 100 GeV. In SUSY GUTs, even without neutrino masses, there is an independent contribution to CLFV, originating from the grouping of quarks and leptons in the same GUT multiplet. The squared masses of the right-handed sleptons would receive contributions to CLFV in this momentum range from the GUT scale particles that are active, given by

$$(m^2_{\tilde{e}_R})_{ij} \simeq -\frac{3}{8\pi^2}V_{3i}V_{3j}^*|Y_t|^2(3m_0^2 + |A_0|^2)\ln\left(\frac{M_{\rm Pl}}{M_{\rm GUT}}\right). \tag{1.7}$$

Here V_{ij} denote the known CKM quark mixing matrix elements, and Y_t is the top quark Yukawa coupling. Unlike Eq. (1.6), which has some ambiguity since Y_ν is not fully known, the CLFV contribution from Eq. (1.7) is experimentally determined, apart from the SUSY parameters.

We next consider RS models with bulk gauge fields and fermions. In these models, our universe is localized on one (ultraviolet) membrane of a multidimensional space while the Higgs field is localized on a different (infrared) membrane. Each particle has a wave function that is localized near the Higgs membrane for heavy particles or near our membrane for light particles. Thus localization of different wave functions between the membranes generates flavor. For a given fermion mass spectrum, there are only two free parameters, an energy scale to set the Yukawa couplings and a length scale of compactification that sets the level of Kaluza-Klein (KK) excitations. The two scales can be accessed using a combination of tree induced CLFV processes that occur in $\mu N \to eN$ or $\mu \to 3e$ and loop induced interactions such as $\mu \to e\gamma$ [**?**, **?**]. The amplitude of loop-induced flavor-changing decays, such as $\mu \to e\gamma$, is given by a positive power of the Yukawa and a negative power of the KK scale. Tree-level flavor-changing diagrams, on the other hand, come from four-fermion interactions whose flavor-changing vertices come from the non-universal profile of an intermediate KK gauge boson. This non-universality is an effect of electroweak symmetry breaking so that the flavor-changing part of the KK gauge boson profile is localized near the IR brane and the size of flavor-changing effects depend on the size of the zero mode fermion profile towards the IR brane. However, in order to maintain the Standard Model fermion spectrum the zero-mode fermion profiles must be pushed away from the Higgs vacuum expectation value on the IR brane as the anarchic Yukawa scale is increased. Thus the tree-level flavor changing amplitudes go like a negative power of the anarchic Yukawa scale. For a given KK scale, experimental constraints on lepton flavor-changing processes at tree and loop level thus set lower and upper bounds on the Yukawa scale, respectively.

A version of minimal flavor violation exists in RS models where the new scales have a very small effect on low energy flavor changing processes. It was noted in [**?**] and [**?**] that certain flavor changing diagrams are suppressed in the RS scenario because the particular structure of zero mode wave functions and Yukawa matrices is the same as the zero mode mass terms induced by electroweak symmetry breaking. When passing to the physical basis of light fermions these processes are also nearly diagonalized, or *aligned*, and off-diagonal elements of these transitions are suppressed. These flavor-changing processes are not completely zero since

the fermion bulk masses are an additional flavor spurion in these theories. In other words, the $U(3)^3$ lepton flavor symmetry is not restored in the limit where the Yukawa terms vanish. The full one-loop calculation of $\mu \to e\gamma$ in Randall-Sundrum models including these misalignment effects and a proof of finiteness was performed in [**?**].

1.2.1.1.1 μ decays

1.2.1.1.2 τ decays

1.2.2 Muon Experimental Overview

1.2.2.1 Muon Flavor Violation Experiments in this Decade

1.2.2.1.1 The Mu2e Experiment

The Mu2e experiment, to be hosted at Fermilab, is a flagship component of the U.S. Intensity Frontier program [1] and will search for the charged-lepton-flavor-violating process of coherent muon-to-electron conversion in the presence of a nucleus ($\mu^- N \to e^- N$). The Mu2e experiment will improve sensitivity compared to current experimental by four orders of magnitude [2] and will set a limit on $R_{\mu e}$, defined as,

$$R_{\mu e} = \frac{\Gamma(\mu^- \, N(A,Z) \to e^- \, N(A,Z)}{\Gamma(\mu^- \, N(A,Z) \to \nu_\mu \, N(A,Z-1))}, \tag{1.8}$$

where $N(A,Z)$ denotes a nucleus with mass number A and atomic number Z. The numerator corresponds to the rate for the CLFV conversion process and the denominator corresponds to the rate for ordinary muon capture on the same nucleus. The current best limit is $R_{\mu e} < 7 \times 10^{-13}$[3].

There is no observable Standard Model contribution to the $\mu^- N \to e^- N$ signal at Mu2e. Neutrino oscillations imply that muon-to-electron conversion can proceed via a penguin diagram that contains a W and an oscillating neutrino. However, the rate for this conversion process is more than 30 orders of magnitude below the projected sensitivity of the Mu2e experiment. Any signal observed at Mu2e would be an unambiguous indication of new physics [4, 5].

The approach of the Mu2e experiment is to stop low-momentum muons from a pulsed beam on an aluminum target to form muonic atoms and then to measure the resulting electron spectrum. The signal would produce a mono-energetic electron with an energy of about 105 MeV. In order to reach the design sensitivity (single-event sensitivity of 2×10^{-17}), about 10^{18} muons must be stopped. Keeping the background expectation to less than one event in this high-intensity experiment is obviously quite a challenge and results in the unique experimental setup summarized below and depicted in Fig. 1-3.

The first step in the experiment is to produce the low-momentum pulsed muon beam. Recycled Tevatron infrastructure will deliver 8 GeV protons with 1695 ns bunch spacing to the experiment, the revolution period of the Debuncher ring. This spacing is well-suited to the Mu2e experiment, given that the lifetime of a muonic aluminum atom is about 864 ns. Pions and muons produced inside the production solenoid are collected and passed to the S-shaped muon beamline where absorbers and collimators are optimized to eliminate positively-charged particles and anti-protons while efficiently transmitting low-energy negatively-charge pions and muons. Most of the pions will decay inside the 13 m long beamline, while about 40%

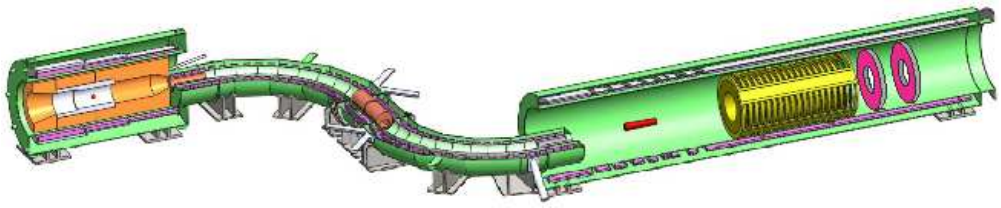

Figure 1-3. *The Mu2e experimental setup. The pulsed proton beam enters the production solenoid (far left) from the top right. Muons produced are captured by the production solenoid and transported through the S-shaped transport solenoid to the aluminum stopping target (small red cylinder). Electrons produced in the stopping target are captured by the magnetic field of the detector solenoid (right) and transported through the tracker (yellow) where the momentum is measured. The electrons then strike the electromagnetic calorimeter (pink annuli), which provides particle identification and an independent measurement of momentum. A cosmic ray-veto system and some other parts of the apparatus are not shown.*

of surviving muons will be stopped in an aluminum stopping target. Simulations estimate that Mu2e will produce 0.0016 stopped muons per proton on target.

Muons stopped in the target form a muonic atom. As they settle into the K-shell a cascade of X-rays will be emitted. By detecting these X-rays the rate of stopped muons can be measured, thereby establishing the denominator of $R_{\mu e}$. About 60% of stopped muons will undergo muon capture on the nucleus while the other 40% will decay in orbit (DIO). The DIO process produces an electron with a continuous Michel distribution including a long tail due to photon exchange with the nucleus. In the limit where the neutrinos carry no energy from the Michel decay, the electron carries the maximum energy of 105 MeV [6]. In this limit, the DIO electron is indistinguishable from the $\mu^- N \to e^- N$ conversion signal. In addition, mis-measurements of the DIO electron momentum contribute to an irreducible background. In order to combat the DIO background, the Mu2e experiment requires a tracking detector with momentum resolution of about 0.1%.

To achieve this momentum resolution, the Mu2e tracker will use straw tubes in vacuum. The inner radius of the tracker is empty so that only tracks with transverse momenta above 53 MeV/c will pass through the straw tubes. The Mu2e scintillating-crystal (LYSO) calorimeter will provide cross checks of signal candidates and particle identification. The calorimeter also has an empty inner-radius region. The empty inner regions effectively make the tracker and calorimeter blind to the bulk of the DIO electrons and to muons that don't stop in the target, and allow these detectors to cope with the high-intensity environment of the experiment.

The primary backgrounds for the Mu2e experiment can be classified into several categories: intrinsic muon-induced backgrounds, late-arriving backgrounds, and miscellaneous backgrounds, primarily anti-proton-induced and cosmic ray-induced backgrounds. The muon-induced backgrounds arise from muon DIO and radiative muon capture. The kinematic endpoint of the electron energy distribution is slightly below 105 MeV, so this background, like the DIO, can be mitigated by minimizing non-Gaussian contributions to the tails of the momentum resolution. The dominant late-arriving background arises from radiative pion capture and subsequent conversion of the γ in the stopping target material to produce a 105 MeV electron. Late-arriving backgrounds like this can be controlled by taking advantage of the long muon lifetime and by optimizing the properties of the pulsed beam. After a beam pulse there is therefore a delay of about 700 ns before the signal timing window begins. In order to avoid late-arriving backgrounds in the signal time window, Mu2e requires the fraction of protons outside the beam pulse to be less than 10^{-10}, which will be achieved and monitored with dedicated systems. Beam electrons, muon decay in flight, and pion decay in flight are other late-arriving backgrounds that are suppressed through the combination of the pulsed beam and delayed signal window.

Cosmic ray muons interacting within the detector solenoid region can produce background electrons. Passive shielding and an active cosmic ray-veto system are employed to ensure that cosmic rays are a sub-dominant background.

The total background expectation in the Mu2e experiment for a three-year run at 8 kW beam power is less than 0.5 events and summarized in Table 1-2.

1.2.2.2 Muon Flavor Violation: The Next Generation

1.2.2.2.1 Mu2e at Project X

Here we summarize a feasibility study [7] of a next-generation Mu2e experiment (Mu2e-II) that uses much of the currently-planned facility and Project-X [8] beams to achieve a sensitivity that is about a factor of ten beyond that of the Mu2e experiment described in Section 1.2.2.1.1. A factor of ten improvement will be interesting regardless of the outcome of Mu2e. If the Mu2e experiment observes events completely consistent with background expectations, then another factor of ten improvement in sensitivity extends the reach to additional beyond-the-standard-model parameter space. If Mu2e observes a 3σ excess, then a Mu2e-II upgrade would be able to definitively resolve the situation. And if Mu2e discovers charged-lepton-flavor-violating physics, then a Mu2e-II upgrade could explore different stopping targets in an effort to untangle the underlying physics. By measuring the signal rate using nuclear targets at various Z, Mu2e-II would have the unique ability to resolve information about the underlying effective operators that are responsible for the lepton-flavor-violating signal [9, 10].

To estimate the signal acceptance and background prediction for Mu2e-II scenarios we use `G4Beamline v2_12` [11], which is a simplified version of Geant4 [12]. Three sets of simulated experiments are studied: the 8 GeV case which corresponds to the Mu2e configuration, and potential Project-X upgrades corresponding to protons with 1 or 3 GeV of kinetic energy. In all instances the full Mu2e solenoid system is simulated including all collimators, the Production Solenoid heat and radiation shield, the antiproton window, and the magnetic field. The stopping target geometry is described in [2] and is left unchanged for the different scenarios.

The timing distribution of the proton pulse in `G4Beamline` is modeled as a delta function located at $t = 0$ ns. In order to get a more accurate estimate of the experimental sensitivity we convolute the relevant timing distributions with the expected shape of the proton pulse as estimated using dedicated simulations of the Mu2e proton beam. For Project-X, the width of the proton pulses are expected to ± 50 ns for 100 kW of beam power [13], which is about a factor of two smaller than what will be used for Mu2e. So, for the Project-X studies we assume the same proton pulse shape as supplied for Mu2e, but reduce the width of the pulse by a factor of two. Most pions decay before reaching the stoping target, and due to this short lifetime it isn't practical to study the pion backgrounds if the decay is simulated. Instead, in these studies all charged pions pions are propagated through to the stopping target and events are weighted by the survival probability.

The stopping-time distributions for muons and pions are studied in Ref. [7] and are used for the estimations of background and signal acceptance below. We find that the stopping-time distributions are largely independent of the stopping target material.

Relevant timing distributions for the Mu2e experiment are shown in the top panel of Fig. 1-4 for an aluminum stopping target. Since the π^--N interaction is strong, the pion capture-time distribution is assumed to be the same as the pion arrival-time distribution. For muons, the capture/decay rate is characterized by a falling exponential. The fractions of bound muons that are captured or that decay-in-orbit (DIO) are also nuclei dependent. These nuclei-dependent characteristics affect the sensitivity of a given experiment and are

	lifetime (ns)	capture fraction	decay fraction
Aluminum	864	0.61	0.39
Titanium	297	0.85	0.15
Gold	72	0.97	0.03

Table 1-1. *The lifetime of the bound muon and the muon capture and decay fractions for various stopping target nuclei that affect the sensitivity estimates for Mu2e-II.*

listed in Table 1-1 for the stopping-target nuclei we considered [14]. The muon decay-time distribution is shown in the top panel of Fig. 1-4 as the blue dashed line. In this figure the timing distributions are folded over modulo 1695 ns in order to account for contributions from previous proton pulses.

The bottom panel of Fig. 1-4 shows the Project-X 3 GeV scenario, where the proton pulse width is half that of the 8 GeV configuration, and both aluminum, titanium, and gold are considered as a stopping target [1]. Because the proton pulse width is narrower, the live gate can be increased in the Project-X scenario [15]. The same exercise was performed for the Project-X 1 GeV scenario and with the exception of the stopping rates, the parameters of the timing distributions for the 1 GeV case are very similar to those of the 3 GeV case. The relavant quantities associated with Fig. 1-4 are included in Ref. [7] and used below to predict the background and signal rates for each scenario.

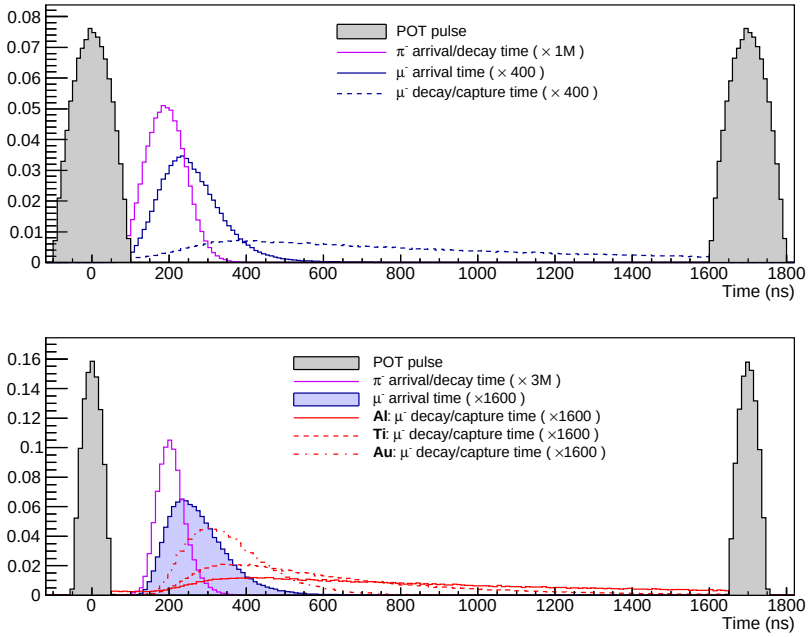

Figure 1-4. *Timing distribution for the 8-GeV Mu2e case (top) and the 3-GeV Project-X case (bottom). Shown here is a figurative POT pulse width, the arrival time of the charged pions and muons, and the decay-time distribution of the muons on aluminum, titanium, and gold.*

We also produced the muon decay-time distribution for a gold stopping target as shown in Fig. 1-4. Since the lifetime of the bound muon is so small (72 ns) the fraction of muon decays/captures that occur within

[1] Note that the arrival times for stopped particles are slightly earlier for titanium than for aluminum although it isn't depicted in the figure.

the live gate is quite small – only 1.22% for a live gate of $670 < t < 1645$ ns. Since the muon decay-time distribution has such a large overlap with the pion arrival time distribution, it's clear that it will be difficult to achieve a reasonable signal acceptance while sufficiently suppressing the RPC background. To achieve the necessary pion/muon separation requires a dedicated study of alternative transport systems and is beyond the scope of this study. We do not further consider the gold stopping target.

We use the quantities from Ref. [7] to estimate the backgrounds for several Mu2e-II scenarios. No additional simulation work was done aside from the simulations described above. Consequently, we here estimate the Mu2e-II backgrounds by scaling from the Mu2e backgrounds which were derived using full simulation as described in [2] and references therein. In numbers quoted in Ref. [7] the stopping rates are larger for titanium than for aluminum due to the fact that in the simulations we left the stopping-target geometry unchanged and that titanium is heavier and at a larger Z. In that configuration a titanium stopping target would also have a poorer momentum resolution. In the estimates below, we assume that reducing the titanium stopping-target mass so that it gave the same stopping rates as aluminum would yield the same momentum resolution. Thus, in these estimates, we always use the aluminum stopping yields for a given proton beam energy and scale from the Mu2e background estimates assuming that the same detector performance for Mu2e-II.

For each beam scenario target nuclei we estimate the number of protons on target ($N_{\rm POT}$) required to improve the signal expectation by a factor of ten. This is done by scaling from the Mu2e experiment by the number of stopped muons per POT, the muon capture fraction, and the fraction of muon capture/decay that occur in the signal timing window. We then take the resulting number of POT and calculate the required beam power, and the number of muon and pion stops per kW, assuming the same run time for Mu2e-II as Mu2e, namely a three-year run with 2×10^7 seconds of run time per year with proton pulse spacing of 1695 ns. These studies predict that between 8.7×10^{21} and 5.3×10^{22} $N_{\rm POT}$ are required depending on the beam and target scenario which corresponds to 70–150 kW of beam power. The detailed results of these calculations are given in Ref. [7].

Several background sources will be reduced or remain minimal at Mu2e-II due to the improved beam characteristics compared to Mu2e. For example, there are no antiproton-induced backgrounds for the Project-X scenarios since both 1 GeV and 3 GeV kinetic energy protons are below the proton-antiproton production threshold. The radiative pion capture background is kept under control for Mu2e-II owing to the narrower proton pulse widths at Project-X and owing to the significantly improved extinction provided by Project-X beams. Late-arriving backgrounds, such as π decay-in-flight, are also kept under control by the decrease in the extinction ratio relative to those same quantities for Mu2e.

The cosmic ray background is independent of $N_{\rm POT}$ and beam power and depends only on the live time of the experiment. Since we assume that Mu2e-II will have the same run time (three-year run with 2×10^7 s/year) and proton pulse spacing (1695 ns) as Mu2e, the only difference is in the duty factor (which increases from 30% to 90%) and the live-gate fraction. We scale the current Mu2e estimate for the cosmic-ray-induced backgrounds to account for these differences. We assume that the veto efficiency for Mu2e-II is unchanged relative to Mu2e (99.99%). For a Project-X (PX) driven Mu2e-II experiment, the resulting cosmic-ray-induced background is 0.16 events.

Some backgrounds scale linearly with the number of stopped muons, such as radiative muon captures and muon decay in orbit, and these can't be mitigated through improved beam characteristics. Radiative muon capture is a negligible background for Mu2e and remains so for Mu2e-II.

The μ decay-in-orbit background is calculated assuming that the probability that a DIO event survives the reconstruction and selection requirements for Mu2e-II are unchanged relative to Mu2e, $\alpha_{\rm DIO} = 1.9 \times 10^{-18}$ [2]. Note that this implicitly assumes that the momentum resolution, and in particular the magnitude and shape

		Mu2e	Mu2e-II	
		8 GeV	1 or 3 GeV	
		Al.	Al.	Ti.
Category	Source		Events	
Intrinsic	μ decay in orbit	0.22	2.14	0.58*
	radiative μ capture	< 0.01	< 0.01	< 0.01
Late Arriving	radiative π capture	0.03	0.04	0.05
	beam electrons	< 0.01	< 0.01	< 0.01
	μ decay in flight	0.01	< 0.01	< 0.01
	π decay in flight	< 0.01	< 0.01	< 0.01
Miscellaneous	antiproton induced	0.10	–	–
	cosmic-ray induced	0.05	0.16	0.16
	pat. recognition errors	< 0.01	< 0.01	< 0.01
Total Background		0.41	2.34	0.79

Table 1-2. *A summary of the current Mu2e background estimates and estimates of how the backgrounds would scale for a next generation Mu2e experiment, Mu2e-II, that employs Project-X beams at 1 or 3* GeV *and an aluminum or titanium stopping target. For a given stopping target, the difference in background yields between a 1* GeV *or a 3* GeV *proton beam is about 10%. The total uncertainty on the total Mu2e background is estimated to be about 20%. We've added a $*$ to the DIO estimate for the titanium stopping target to emphasize the fact that this number is expected to change once more detailed studies have been completed [16].*

of the high-side tail, is unchanged relative to Mu2e. In addition, it assumes that the shape of the DIO spectrum for a titanium stopping target is the same as the shape of the spectrum for aluminum stopping target. A Mu2e-II experiment with an aluminum stopping target and a $\times 10$ better sensitivity than Mu2e is therefore expected to have a DIO background $\times 10$ larger than Mu2e. The only mitigations are to make more stringent momentum requirements or to redesign the tracker and the upstream material (e.g. stopping target, internal proton and neutron absorbers, etc.) to improve the momentum resolution. Studies of the DIO background performed for the Mu2e experiment show that it is unlikely that for an aluminum stopping target, more stringent selection requirements alone could mitigate a ten-fold increase in the DIO background without a significant reduction in signal sensitivity. For the increased sensitivity of a Mu2e-II experiment an improved momentum-scale calibration may also be required to reduce the DIO background. This would not necessarily be the case for a Mu2e-II experiment that uses a titanium stopping target [16].

The summary of the background estimates for Mu2e-II are given in Table 1-2 along with the estimate for Mu2e.

Several components of the Mu2e experiment may need to be upgraded to handle the higher rates and physics requirements of Mu2e-II. To accommodate beam power in the 80kW-110kW range estimated for Mu2e-II several aspects of the Target and Target Hall would have to be upgraded. The proton beam dump would need improved cooling and the production target would need to be redesigned. A new production target design would likely require modifications to the remote target handling system. Depending on the proton beam energy and the PS configuration, it may be necessary to redesign some portions of the Mu2e beam line just upstream of the PS. Since the extinction in the Project-X scenarios is a factor 100 smaller than for Mu2e, the Extinction Monitor system would have to be upgraded to increased acceptance/sensitivity. It is expected that even at the increased rates and beam power discussed earlier, the transport solenoid and

detector solenoid should be able to operate reliably for a Mu2e-II run. For the production solenoid, the limiting factors are the peak power and radiation damage it would incur at the increased beam power. For example, the Production Solenoid heat and radiation shield , which is currently planned to be fabricated from bronze, could sustain higher peak power if replaced with tungsten [7].

Although the beam power increases by a factor of 10 or more, the instantaneous rates only increase by a factor of 3-5 owing to the increased duty factor expected from Project-X. This has important consequences for the viability of reusing much of the currently planned Mu2e detector apparatus for a next generation Mu2e-II. For example, the current Mu2e tracker is being designed to handle instantaneous rates higher than what is currently estimated. Simulation studies in which the instantaneous rates are increased by factors of two or four have been performed. These studies indicate that at four times the nominal rates the tracker reconstruction efficiency only falls by about 5% while maintaining the same momentum resolution. Thus, these studies indicate that the Mu2e tracker would be able to handle the Project-X rates. Simulation studies are necessary to quantify the degree to which the increased rates affect the calorimeter's performance. If it turns out that the expected performance is not sufficient to meet the Mu2e-II physics requirements, then it may be necessary to upgrade to faster readout electronics or to a faster crystal (*e.g.* BaF_2). Regardless of the outcome of the simulation studies, the photo sensors will likely require replacement owing to radiation damage incurred during Mu2e running. The performance of the LYSO crystals is not expected to be significantly affected by the radiation dose incurred during Mu2e running.

The current design of the cosmic ray veto system should be adaptable to the case with a factor of 3–5 increase in rate with only minor upgrades required and these may only be needed in the most intense radiation regions of the veto system. Experience from the first run of the Mu2e experiment will be crucial in quantifying limitations of the system for future intensity upgrades. Improved shielding will likely be required in the highest radiation regions to reduce incidental rates in the veto counters.

We investigated the feasibility of a next generation Mu2e experiment (Mu2e-II) that uses as much of the currently planned facility as possible and Project-X beams to achieve a sensitivity that's about a factor of ten better than Mu2e. Based on these studies we conclude that a Mu2e-II experiment that reuses a large fraction of the currently planned Mu2e apparatus and provides a $\times 10$ improved sensitivity is feasible at Project-X with 100-150 kW of 1 or 3 GeV proton beams. Aside from the DIO background, which requires improved momentum resolution to mitigate, the remaining backgrounds are kept under control due to important features of Project-X. The narrower proton pulse width and expected excellent intrinsic extinction are both important to mitigating the RPC background. The excellent intrinsic extinction is also important in mitigating backgrounds from late arriving protons such as μ and π decay-in-flight and beam election backgrounds. A beam energy below the proton-antiproton production threshold eliminates the antiproton induced backgrounds. The high duty factor expected for Project-X is important since it enables a ten-fold improvement in sensitivity over a reasonable timescale while necessitating only a modest increase (a factor of 3-5, depending on scenario) in instantaneous rates at the detectors. Because the instantaneous rates increase only modestly, we believe that Mu2e-II could reuse the currently planned Mu2e apparatus with only modest upgrades necessary.

1.2.2.2.2 A surface μ^+ Beam

The production of muons typically proceeds through the interaction of a proton beam in a target where positive and negative pions are created. Their decays generate positive and negative muons that can be collected in a subsequent secondary beamline in order to provide the muon beam to the experimental setup. In most cases, the muons are stopped in a target material at the center of the detection system. Experiments searching for charged lepton flavor violating (CLFV) decay channels of the muon such as $\mu \to e\gamma$ or $\mu \to eee$

require the precise reconstruction four momentum of the decay products. For that reason, the muon stopping target should be as thin as possible to suppress multiple scattering for the decay products. On the other side, the target's thickness determines the stopping efficiency of muons. The range R_μ of a muon beam with momentum p is proportional to $p^{3.5}$. The total range spread ΔR_μ of the stopped muons in a target is given by the momentum spread Δp of the beam and a constant term due to the range straggling [24]:

$$\frac{\Delta R_\mu}{R_\mu} = \sqrt{\left(3.5\frac{\Delta p}{p}\right)^2 + (0.1)^2}.$$

A lower beam momentum is hence favorable to increase the stopping density of the muons allowing to minimize the target thickness.

The pions produced in the proton target provide two distinct sources for muons: i) so-called surface (and sub-surface) muons and ii) cloud muons. The surface muons originate from pions that stop near the surface of the proton target. Due to the fixed kinematics of the two body decay $\pi^\pm \to \mu^\pm \nu_\mu$ at rest, the outgoing muon has a fixed momentum of 29.8 MeV/c. Surface (and sub-surface) muons hence have momenta below this specific momentum depending on the pion's decay location inside the target. If the pion has enough momentum to escape the proton target, its decay in flight produces muons with momenta exceeding 29.8 MeV/c. These muons are called cloud muons as they have their origin in the moving pions near the target surface. The left panel of Figure 1-5 shows the predicted production rates of pions (red) and muons (green) for the $\pi E5$ beamline at the Paul Scherrer Institute (PSI) in Switzerland. A clear surface muon peak in the μ^+ yields just below the momentum of 29.8 MeV/c is visible. Since negative pions undergo nuclear capture if stopped in the target, negative surface muons are not produced. Cloud muons rates scale typically with p^3 due to a constant momentum bite of the muon beamline channel and the phase space scaling with p^2 [27]. The Figure also shows that positive particle rates exceed the negative particle rates due to the positive charge of the proton beam.

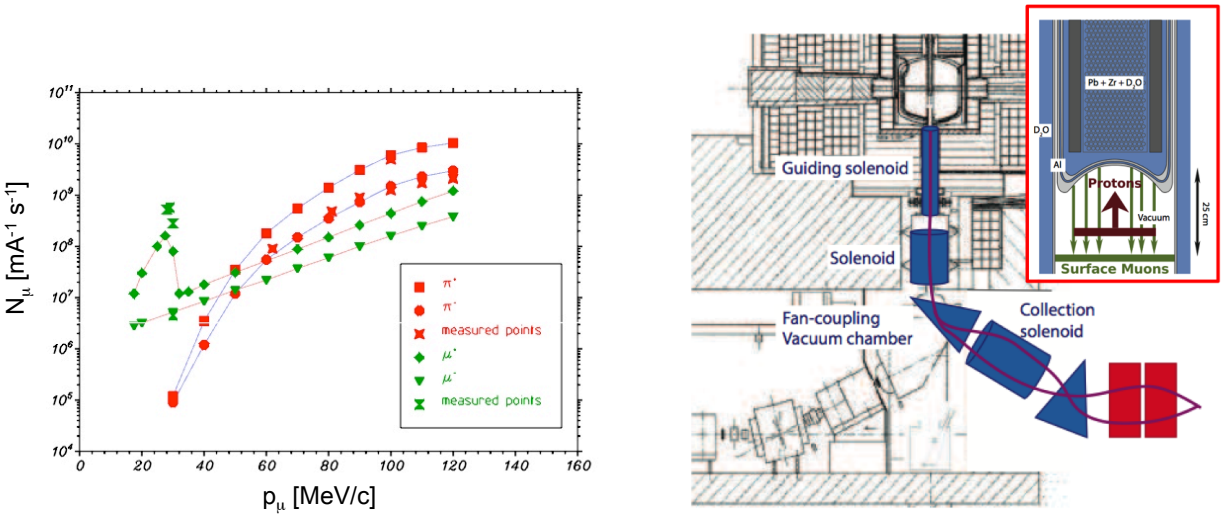

Figure 1-5. *Left panel: Pion and muon rates versus particle momentum for both charges predicted for the $\pi E5$ beamline at PSI together with a few measured data points. Right panel: Conceptual design of a possible high intensity muon beamline at the spallation source target at PSI. Red inlet is a zoom of the neutron target region.*

The high rates of surface (and sub-surface) positive muons and their low momentum leading to a high stopping density as explained above make these an ideal choice for the searches of CLFV via $\mu^+ \to e^+\gamma$

or $\mu^+ \to e^+e^+e^-$. Other physics experiments such as the MuLan experiment [26] also relied on surface muon beams due to the high rates while employing a thin stopping target. Table 1-3 shows some examples of finalized and future particle physics experiments that all use surface muons (except for the future Mu2e experiment at FNAL which requires negative muons). From the beam rates column one can see that future experiments require the next generation surface muon beams with rates of an order of magnitude larger than the current available maximum rates at PSI.

Table 1-3. *Overview of some muon experiments and their beam parameters. Experiment marked with * are future experiments.*

Experiment	**Beam**	**Momentum [MeV/c]**	**Rates [s^{-1}]**	B**Beamline**
MEG ($\mu \to e\gamma$) [18]	μ^+	29.8	$3 \cdot 10^7$	πE5 at PSI
MuLan [26]	μ^+	29.8	$8 \cdot 10^6$	πE3 at PSI
TWIST [23]	μ^+	29.8	$< 5 \cdot 10^3$	TRIUMF
MEG upgrade* ($\mu \to e\gamma$) [30]	μ^+	29.8	$7 \cdot 10^7$	πE5 at PSI
Mu2e* ($\mu^- \to e^-$) [17]	μ^-	~ 40	10^{10}	FNAL
$\mu^+ \to e^+e^-e^+$ (Phase 1)* [20]	μ^+	29.8	$< 1 \cdot 10^8$	πE5 at PSI
$\mu^+ \to e^+e^-e^+$ (Phase 2)* [20]	μ^+	29.8	$2 \cdot 10^9$	HIMB at PSI

In addition to the listed particle and nuclear physics experiments in Table 1-3, surface muon beams are highly polarized making them very suitable for material science applications via the Muon Spin Rotation (muSR) technique. Several facilities worldwide currently provide surface muon beams. Table 1-4 shows the two laboratories (PSI, J-PARC, and RCNP Osaka University) with the currently highest rates of up to a few $10^8\,s^{-1}$ as well as future estimated rates including a possible facility at Fermilab with Project-X beams. Other facilities like TRIUMF, KEK, RAL-ISIS, and Dubna have rates $< 10^7\ s^{-1}$ and were omitted in this table.

Next generation CLFV experiments with a surface muon beam ($\mu^+ \to e^+\gamma$ [30] and $\mu^+ \to e^+e^-e^+$ [20]) are in the design and planning stages at PSI. Since these experiments have to suppress accidental backgrounds which scale with the square of the beam rate, they require continuous beams. The current πE5 beamline at PSI with conventional focusing quadrupole elements can deliver about $2 \cdot 10^8$ muons/s at the proton beam power of 1.3 MW. However, this beamline views target station E [22] at PSI where only about 20 % of the proton beam interacts. Most of the beam is transmitted to the neutron spallation target at the end of the proton beamline. PSI is currently studying the possibility of a high instensity muon beamline (HIMB) at the neutron spallation target based on a large capture solenoid concept. The conceptual design is shown in the right panel of Figure 1-5. About 70 % of the 1.3 MW proton beam is coming from the left and directed upwards into the SINQ target of lead-filled zircaloy tubes surrounded by a cooling D_2O layer. Surface muons from the aluminum window (see red framed inlet) could then be collected in the downwards direction with newly installed solenoids (blue) into a new dedicated new beamline. Realistic Monte Carlo simulations give an estimate of about $1 \cdot 10^{11}$ muons/s below 29.8 MeV/c corresponding to a rate of $3 \cdot 10\,s^{-1}$ for 10 % momentum bite around 28 MeV/c [20].

Table 1-4 also shows the different beam energies at the 3 facilities. While PSI employs a DC, 590 MeV proton beam of about 1.3 MW total power, J-PARC (pulsed mode) and Fermilab with its future Project-X[2]

[2] http://projectx.fnal.gov/

Table 1-4. *Summary of some current and planned muon beam facilities at various worldwide laboratories. Table reproduced in parts from [20]*

Laboratory / Beam Line	Energy / Power	Present Surface μ^+ rate (Hz)	Future estimated μ^+/μ^- rate (Hz)
PSI (CH)	(590 MeV, 1.3 MW, DC)		
LEMS	"	$4 \cdot 10^8$	
πE5	"	$1.6 \cdot 10^8$	
HiMB	(590 MeV, 1 MW, DC)		$4 \cdot 10^{10}(\mu^+)$
J-PARC (JP)	(3 GeV, 1MW, Pulsed)		
	currently 210 KW		
MUSE D-line	"	$3 \cdot 10^7$	
MUSE U-line	"		$2 \cdot 10^8(\mu^+)(2012)$
COMET	(8 GeV, 56 kW, Pulsed)		$10^{11}(\mu^-)(2019/20)$
PRIME/PRISM	(8 GeV, 300 kW, Pulsed)		$10^{11-12}(\mu^-)(> 2020)$
FNAL (USA)			
Mu2e	(8 GeV, 25 kW, Pulsed)		$5 \cdot 10^{10}(\mu^-)(2019/20)$
Project X Mu2e	(3 GeV, 750 kW, DC to pulsed)		$2 \cdot 10^{12}(\mu^-)(> 2022)$

accelerator infrastructure (DC and pulsed mode) have 3 GeV beams eith about 1 MW of power. Original studies at ISIS [21] found that the muon yields per MW of beam power are 3-7 times lower at 3 GeV compared to PSI's 590 MeV. However, recently corrected pion cross sections in GEANT4 demonstrated that the yields are rather similar [25]. Therefore, an optimized surface muon beamline in the Project-X era at Fermilab with 750 kW beam power could be a competetive option to a HIMB development at PSI.

As described in the following sections, the feasibility of next generation experiments ($\mu^+ \to e^+\gamma$ and $\mu^+ \to e^+e^-e^+$) would require the availability of a high rate (sub-)surface muon beam. With the prospect of the high power 3 GeV beams at Project-X surface muon beams could become available to a multitude of applications at Fermilab such as particle physics and material science with muSR. Besides the available beam power of about 750 kW for a muon program, the flexibility of the accelerator beam structure is an additional benefit to serve a multitude of experiments with different requirements. The design of a future surface muon beamline will need to take into account a variety of parameters for the optimization:

- Proton target: The design of the proton target by itself has many design parameters. The target can either be at the end of the proton beamline in conjunction with a planned neutron spallation target similar to aforementioned HIMB strategy at PSI. Alternatively, the proton target could be in the proton beam and only using a fraction of the available beam. The material choice and target shape influence the surface muon yields, mechanical stability and determine the cooling requirements. Other aspects of the design include the minimization of secondaries (e.g. $e^{\pm}$, $\pi^{\pm}$, γ, and n) and ideally a low activation throughout operation.
- Muon beam channel: The development of a specific concept of the muon beam channel should be based on the experimental requirements such as required muon rates, polarization, momentum and momentum bite as well as the beam spot at the stopping target. As mentioned before, there are two major concepts based on either a more conventional design with focusing quadrupole elements or large

solid angle capture solenoids. Specific elements such as a $E \times B$ separator will influence the beam contamination with electrons and the length of the beamline and pulsed mode are important for the remaining pion flux.

- The muon stopping target: While this element is not necessarily part of the beam channel design, it is yet necessary to include its optimization together with the available tuning parameters of a beamline (such as momentum, momentum bite and beam spot). Design parameters include the target material and shape.

Alternatively to a dedicated new surface muon beamline(s) at Project-X that could serve both the next generation particle physics experiments and a muSR user community, one should also investigate in more details whether the future Mu2e proton target and capture solenoids could be adapted for a surface muon beam. Very first Monte Carlo simulations indicate that surface muons would be transported through the solenoids and might be efficiently stopped in a thin walled tubular target. For pion suppression, the Mu2e setup operates in pulsed mode which is not ideal for experiments like $\mu^+ \to e^+\gamma$ and $\mu^+ \to e^+e^-e^+$ as explained above due to the accidental backgrounds. While a simple estimate of a pulsed mode only shows a slight loss compared to an ideal DC beam, a detailed investigation with a full simulation is required to compare an adapted Mu2e beamline to a dedicated surface muon facility. In addition, the current Mu2e setup does not include a separator for electron suppression.

In summary, the prospect of a high power 3 GeV proton beam available for a future muon program at Project-X offers the opportunity to provide a world leading surface muon beam competitive with the rates at other facilities (specifically the planned HIMB beamline at PSI). This could facilitate the next generation of CLFV experiments in addition to a material science oriented muSR facility. However, given the variety of optimization parameters, the development of a concept would require significant Monte Carlo and other design studies.

1.2.2.2.3 $\mu \to e\gamma$

The current limit on the $\mu^+ \to e^+\gamma$ branching fraction is 5.7×10^{-13} at 90% confidence level from MEG at PSI [28], using 3.6×10^{14} stopped muons, from data taken in 2009–2011. Their sensitivity is dominated by accidental background, which is related to the muon stop rate R_μ and various experimental resolutions [30]:

$$N_{\rm acc} \propto R_\mu^2 \times \Delta E_\gamma^2 \times \Delta P_e \times \Delta\Theta_{e\gamma}^2 \times \Delta t_{e\gamma} \times T, \tag{1.9}$$

where $\Delta t_{e\gamma}$, ΔP_e, ΔE_γ, and $\Delta\Theta_{e\gamma}$ are the resolutions of detector timing, positron momentum, photon energy, and positron-photon angle, respectively, and T is total data acquisition time. MEG will conitnue taking data through 2013. They expect to approximately double their published dataset [**?**].

The MEG upgrade plans to improve the experiment sensitivity by a factor of 10. They will increase the intensity of the surface beam, and use a thinner or active stopping target. The detector upgrade includes a larger drift chamber with thinner wires and smaller cells, an improved timing counter, and a larger LXe calorimeter with SiPM readout. Data-taking is planned in the years 2016–2019.

The photon energy resolution is a limiting factor in a $\mu^+ \to e^+\gamma$ search. A pair spectrometer, based on reconstruction of e^+e^- pair tracks produced in a thin converter can provide improved photon energy resolution, at a sacrifice in efficiency. Even though only a small fraction of photons will convert, the much higher power beam at Project X can compensate for the loss of statistics [29]. The thickness of the converter affects the energy resolution due to multiple scattering. Aa detailed study is thus required to prove that this approach does indeed provide an overall improvement, as well as to optimize the converter thickness and to study the utility of making the converter active.

We have conducted an initial study of this concept using a fast simulation tool (FastSim) originally developed for the Super$B$ experiment using the *BABAR* software framework and analysis tools. FastSim allows us to model detector components as two-dimensional shells of simple geometries. Particle scattering, energy loss, secondary particle production (due to Compton scattering, Bremsstrahlung, conversion, EM or hadron showers, *etc.*) are simulated at the intersection of particles with detector shells. Tracks are reconstructed with a Kalman filter into piece-wise trajectories.

The FastSim model consists of a thin aluminum stopping target and a six-layer cylindrical silicon detector. A 0.56 mm thick lead (10% X_0) half cylinder covering 0–π in azimuthal angle at $R = 80$ mm serves as the photon converter. The target consists of two cones connected at their base; each cone is 30 mm high, 5 mm in radius, and 50 μm thick. Two silicon detector cylinders are placed close the target for better vertexing resolution; two layers are placed just outside the Pb converter, and two layers a few cm away. The layout is shown in Fig. 1-6. The entire detector is placed in a 1 T solenoidal magnetic field.

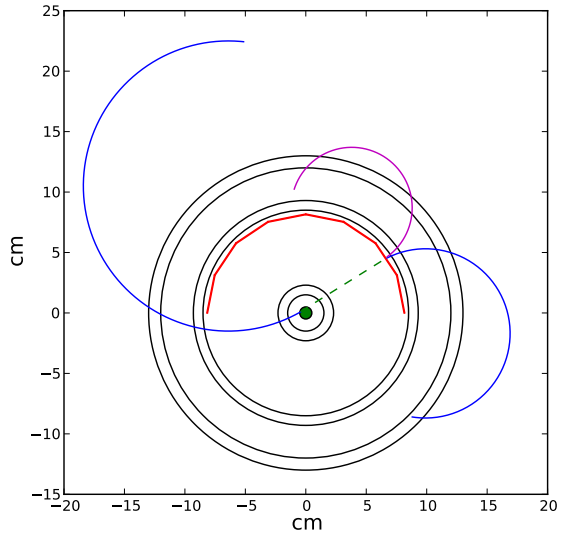

Figure 1-6. *Schematic drawing (x-y view) of the $\mu \to e\gamma$ detector used in the FastSim model.*

We generate muons at rest and let them decay via $\mu^+ \to e^+\gamma$ to study the reconstruction efficiency and resolution. Approximately 1.3% of generated signal events are well-reconstructed, passing quality and fiducial selections criteria. The photon energy resolution is approximately 200 keV, similar to the positron momentum resolution, which corresponds to 0.37% for 52.8 MeV photons. This is a great improvement compared to the 1.7%–2.4% resolution of the current MEG and the 1.0%–1.1% resolution goal of the MEG upgrade. The muon candidate mass resolution is 340 keV (85% Gaussian core). Figure 1-7 shows the photon energy and muon candidate mass resolutions. The positron energy resolution is better than that of MEG, but not as good as what is expected in the MEG upgrade. Angular resolution is similar to the current MEG.

Using a converted photon to increase the $\mu^+ \to e^+\gamma$ detection sensitivity thus appears to be a promising approach. Further studies are needed to quantify the requirements to improve upon the MEG upgrade sensitivity by an order of magnitude or more.

An alternative version of the photon conversion approach to a $\mu \to e\gamma$ experiment has also been discussed. In this version, consider a large volume solendoidal magnet, such as the KLOE coil, which has a radius of

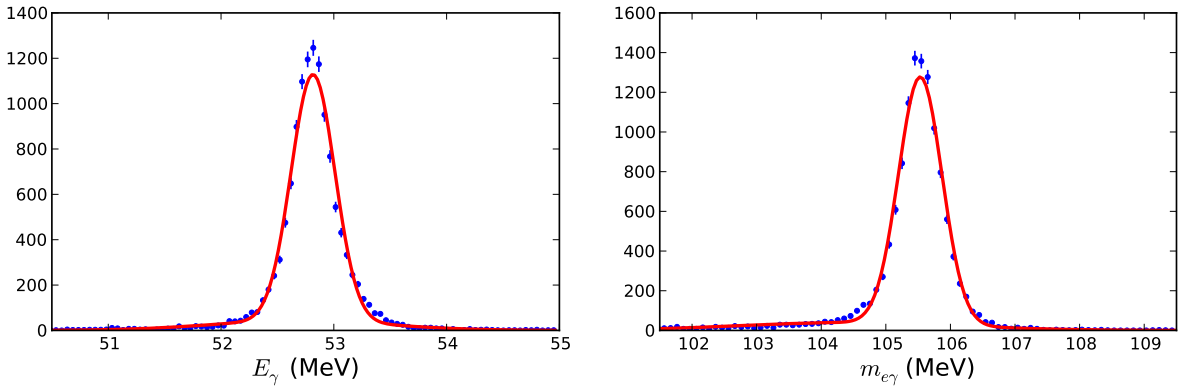

Figure 1-7. *Photon energy and muon candidate mass resolutions in $\mu^+ \to e^+\gamma$ FastSim study. Fitted curve is a double-Gaussian distribution.*

2.9m, run at a field of perhaps 0.25T. A large volume, low mass cylindrical drift chamber provides many ($\geq$100) layers of tracking, utilizing small cells and having a total number of sense wires approaching 10^5. Interspersed every ten layers is a 0.5 mm W converter shell. There are a sufficient number of points on the e^+ and e^- tracks from converted photons behind each converter to reach a total conversion efficiency of perhaps 80%, with excellent photon mass resolution.

1.2.2.2.4 $\mu \to 3e$

1.2.2.2.5 Muonium $\to$ anti-muonium

1.2.3 Tau Experimental Overview

In contrast to muon CLFV searches, in which a single dedicated experiment is required for a given decay, τ lepton CLFV searches are conducted using the large data sets collected in comprehensive e^+e^- or hadron collider experiments. The relative theoretical parameter reach of μ and τ decay experiments is model-dependent, and thus comparisons of limits or observations in the two cases can serve to distinguish between models. Tests with taus can be more powerful on an event-by-event basis than those using muons, since the large τ mass greatly decreases Glashow-Iliopoulos-Maiani (GIM) suppression, correspondingly increasing new physics partial widths (typically by a factor of $\geq$ 500 in $\mathcal{B}(\tau \to \mu\gamma)$ or $e\gamma$ *vs.* $\mathcal{B}(\mu \to \rceil\gamma)$). The difficulty is that one can typically produce $\sim 10^{11}$ muons per second, while the samples from *BABAR* and Belle collected over the past decade together total $\sim 10^{10}$ events.

The new generation of super B or τ/c factories, [**?**] promise to extend the experimental reach in τ decays to levels that sensitively probe new physics in the lepton sector. Since CLFV is severely suppressed in the Standard Model, CLFV τ decays are especially clean probes for New Physics effects. The super flavor factories can access τ CLFV decay rates two orders of magnitude smaller than current limits for the cleanest channels (*e.g.*, $\tau \to 3\ell$), and at least one order of magnitude smaller for other modes that have irreducible backgrounds, such as $\tau \to \ell\gamma$. Super flavor factories thus have a sensitivity for CLFV decays that directly confronts many NP models.

Polarized beams at an e^+e^- collider can provide further experimental advantages. Belle II at SuperKEKB will not have a polarized beam, but both the proposed BINP and Tor Vergata τ/c factories will have polarized electron beams. Polarization of the taus thus produced provides several advantages. It allows reduction of backgrounds in certain CLFV decay modes, as well as providing sensitive new observables that increase precision in other important measurements, including searches for *CP* violation in τ production and decay, the measurement of $g-2$ of the τ, and the search for a τ EDM. Preliminary studies indicate that polarization improves the sensitivity on these quantities by a factor of two to three. Should the CLFV decay $\tau \to 3\ell$ be found, a study of the Dalitz plot of the polarized τ decay can determine the Lorentz structure of the CLFV coupling.

The provision of polarization requires a polarized electron gun, a lattice that supports transverse polarization at the desired CM energy, a means of interchanging transverse polarization in the ring and longitudinal polarization at the interaction point and a means of monitoring the polarization, typically a Compton polarimeter to monitor the backscattering of circularly polarized laser light. Achieving useful longitudinal polarization at the interaction point requires sufficiently long depolarization time of the machine lattice, which is highly dependent on the details of the lattice and the beam energy.

Provision of a polarized positron beam is difficult and expensive; it is generally also regarded as unnecessary, as most of the advantages of polarization for the measurements cited above can be accomplished with a single polarized beam.

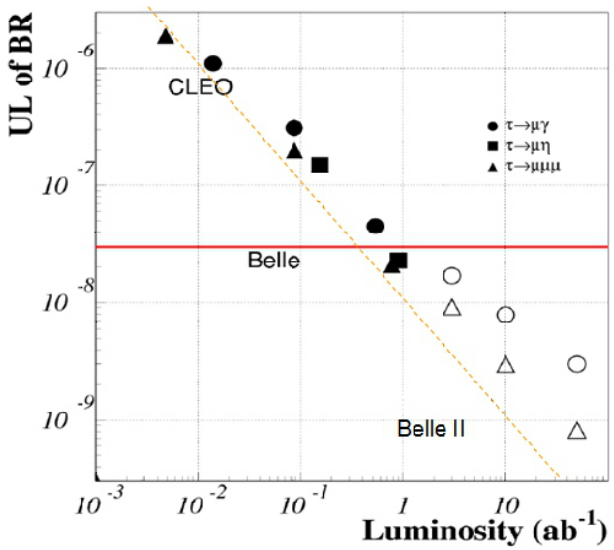

Figure 1-8. *Extrapolationn of the 90% upper limit sensitivity of Belle-II (open symbols) from existing limits (filled symbols). For $\tau \to \mu\gamma$, which has irreducible backgrounds, the limit scales as $1/\sqrt{\int \mathcal{L}dt}$. For $\tau \to \mu\mu\mu$, which is essentially background-free, the limit scales as $1/\int \mathcal{L}dt$.*

The sensitivity of τ CLFV searches at SuperKEKB has been estimated by extrapolating from current CLEO, Belle and *BABAR* limits (see Figure 1-8 The optimization of search sensitivities depends on the size of the sample as well as on the sources of background. For SuperKEKB, the extrapolation for the (largely background-free) $\tau \to \ell\ell\ell$ modes assumes $1/\mathcal{L}$ scaling up to 5 ab^{-1}; that for $\tau \to \ell\gamma$ modes scales as $1/\sqrt{\mathcal{L}}$. The expected sensitivities for several modes are shown for the Belle II experiment in Table 1-5 [**?**].

These CLFV sensitivities directly confront a large variety of new physics models. Of particular interest is the correlation between τ CLFV branching ratios such as $\tau \to \mu\gamma$ and $\tau \to e\gamma$, as well as the correlation with $\mu \to e\gamma$ and the $\mu \to e$ conversion rate, all of which are diagnostic of particular models. A polarized electron beam potentially allows the possibility of determining the helicity structure of CLFV couplings from Dalitz plot analyses of, for example, $\tau \to 3\ell$ decays.

The experimental situation at a τ/c factory is somewhat different. The luminosity of the proposed projects is $10^{35}\text{cm}^{-2}\text{s}^{-1}$, a factor of eight below the eventual SuperKEKB luminosity. The τ production cross section is, however, larger: $\sigma_{\tau\bar{\tau}}(3.77\text{ GeV})/\sigma_{\tau\bar{\tau}}(10.58\text{ GeV}) = 3$, and both have a polarized electron beam. In addition, while a Super B factory is likely to spend the bulk of its running time at the $\Upsilon(4S)$, a τ/c factory will take data more evenly throught the accessible energy range. A study for the BINP machine, with 1.5 ab^{-1} at 3.686 GeV, 3.5 ab^{-1} at 3.770 GeV, and 2.0 ab^{-1} at 4.170 GeV, corresponding to 2.5×10^{10} produced τ pairs, quotes a 90% confidence level limit on $\mathcal{B}(\tau \to \mu\gamma) = (3.3 \times 10^{-10})$, provided the detector has μ/π rejection of a factor of 30. This is nearly an order of magnitude improvement over the SuperKEKB expectation at 50 ab^{-1}.

The experimental discrepancy with the Standard Model prediction for the muon anomalous magnetic moment heightens interest in the possibility of measuring $g-2$ of the τ lepton using angular distributions in τ-pair production. This can be done at a super flavor factory, with or without electron polarization.

The best current bound on the τ anomalous moment $a_\tau = (g-2)/2$ is indirect, derived from the LEP2 measurement of the total cross section for $e^+e^- \to e^+e^-\tau^+\tau^-$: $-0.052 < a_\tau < 0.013$ @ 95% CL. This is well above the Standard Model prediction: $a_\tau^{SM} = 1177.21(5)\times10^{-6}$, but even so provides a model-independent bound on New Physics contributions: $-0.007 < a_\tau^{NP} < 0.005$ @ 95% CL. [G.A. Gonzàlez-Sprinberg, A. Santamaria, J. Vidal, Nucl. Phys. B 582 (2000) 3.]

This measurement can be done in $e^+e^- \to \tau^+\tau^-$ production with unpolarized beams. Determination of the real part of the form factor reuqires the measurement of correlations between the decay rpoducts of of

With polarized taus one can access new observables that are estimated by Bernabéu *et al.*[**?**] to increase the sensitivity to $g-2$ by a factor of three, to $\sim 2\times10^{-6}$ with 80% electron polarization, which could allow a measurement of the Standard Model moment to a precision of several percent with a data sample of 75 ab^{-1}.

Observation of a τ EDM would be evidence of T violation. T-odd observables can be isolated by the study of τ angular distributions using unpolarized beams. Having a polarized electron beam allows these investigations to be done using the decay products of individual polarized taus. The upper-limit sensitivity for the real part of the τ EDM has been estimated to be to be $|\mathcal{R}e\, d_\gamma| \simeq 3\times10^{-19}\ e\cdot\text{cm}$ with 50 ab^{-1} at Belle II and $|\mathcal{R}e\, d_\gamma| \simeq 7\times10^{-20}\ e\cdot\text{cm}$ with 75 ab^{-1} at Super$B$[**?**].

Table 1-5. *Expected* 90% *CL upper limits on* $\tau \to \mu\gamma$, $\tau \to \mu\mu\mu$, *and* $\tau \to \mu\eta$ *with* 5 ab^{-1} *and* 50 ab^{-1} *data sets from Belle II and Super KEKB.*

Process	5 ab^{-1}	50 ab^{-1}
BR($\tau \to \mu\,\gamma$)	10×10^{-9}	3×10^{-9}
BR($\tau \to \mu\,\mu\,\mu$)	3×10^{-9}	1×10^{-9}
BR($\tau \to \mu\eta$)	5×10^{-9}	2×10^{-9}

A *CP*-violating asymmetry in τ decay would be manifest evidence for physics beyond the Standard Model. *BABAR* has recently published a 3σ asymmetry in $\tau \to \pi K^0_S (\geq 0\pi^0)$ decay[**?**]. The super flavor factories have the sensitivity to definitely confirm or refute this measurement, and, further, provide access to new *CP*-odd observables that increase the sensitivity in the search for a *CP* asymmetry to the level of $\sim 10^{-3}$.

1.2.3.1 Super B Factory

1.2.3.2 τ-charm Factory

1.2.3.3 Leptoquark ($e \to \tau$) search

1.3 Flavor-Conserving Processes

1.3.1 Magnetic and Electric Dipole Moment Theory Overview

The muon provides a unique opportunity to explore the properties of a second-generation particle with great precision. Several muon properties make these measurements possible. It has a long lifetime of $\simeq 2.2$ μs, it is produced in the weak decay $\pi^- \to \mu^- \bar{\nu}_\mu$ providing copious numbers of polarized muons, and the weak decay $\mu^- \to e^- \nu_\mu \bar{\nu}_e$ is self-analyzing providing information on the muon spin direction at the time of decay.

In his famous paper on the relativistic theory of the electron, Dirac[31] obtained the correct magnetic moment for the electron, and he also mentioned the possibility of an electric dipole moment, which like the magnetic dipole moment, would be directed along the electron spin direction. The magnetic dipole (MDM) and electric dipole (EDM) moments are given by

$$\vec{\mu} = g\left(\frac{Qe}{2m}\right)\vec{s}, \qquad \vec{d} = \eta\left(\frac{Qe}{2mc}\right)\vec{s}, \tag{1.10}$$

where $Q = \pm 1$ and $e > 0$. Dirac theory predicts $g \equiv 2$, but radiative corrections dominated by the lowest-order (mass-independent) Schwinger contribution $a_{e,\mu,\tau} = \alpha/(2\pi)$ [32] make it necessary to write the magnetic moment as

$$\mu = (1+a)\frac{Qe\hbar}{2m} \quad \text{with} \quad a = \frac{g-2}{2}. \tag{1.11}$$

The muon played an important role in our discovery of the generation structure of the Standard Model (SM) when experiments at the Nevis cyclotron showed that g_μ was consistent with 2 [33]. Subsequent experiments at Nevis and CERN showed that $a_\mu \simeq \alpha/(2\pi)$ [34, 35], implying that in a magnetic field, the muon behaves like a heavy electron. The SM value of the muon anomaly is now known to better than half a part per million (ppm), and has been measured to a similar precision [36].

The quantity η in Eq. 1.10 is analogous to the g-value for the magnetic dipole moment. An EDM violates both P and T symmetries [37, 38, 39], and since C is conserved, *CP* is violated as well. Thus searches for EDMs provide an important tool in our quest to find non-Standard Model *CP* violation.

The measured value of the muon anomalous magnetic moment is in apparent disagreement with the expected value based on the SM. The BNL E821 experiment finds [40]

$$a_\mu(\text{Expt}) = 116\,592\,089(54)(33) \times 10^{-11}, \tag{1.12}$$

where $a_\mu = (g-2)/2$ is the muon anomaly, and the uncertainties are statistical and systematic, respectively. This can be compared with the SM prediction [41, 42]

$$a_\mu(\text{SM}) = 116\,591\,802(42)(26)(02) \times 10^{-11}, \tag{1.13}$$

where the uncertainties are from the $\text{O}(\alpha^2)$ hadronic vacuum polarization (HVP) contribution, $\text{O}(\alpha^3)$ hadronic contributions (including hadronic light-by-light (HLbL) scattering), and all others (pure QED, including a 5-loop estimate [43], and electroweak, including 2-loops [44]). The hadronic contributions dominate the uncertainty in $a_\mu(\text{SM})$. The discrepancy between the measurement and the SM stands at

$$\Delta a_\mu = 287(80) \times 10^{-11} \tag{1.14}$$

(3.6 standard deviations (σ)), when based on the $e^+e^- \to$ hadrons analysis for the HVP contribution [41]. When the HVP analysis is complemented by $\tau \to$ hadrons, the discrepancy is reduced to 2.4σ [41]. However, a recent re-analysis, employing effective field theory techniques, of the τ data [45] shows virtual agreement with the e^+e^--based analysis, which would solidify the current discrepancy at the 3.6σ level. Δa_μ is large, roughly two times the EW contribution [44], indicating potentially large new physics contributions.

The anomalous magnetic moment of the muon is sensitive to contributions from a wide range of physics beyond the standard model. It will continue to place stringent restrictions on all of the models, both present and yet to be written down. If physics beyond the standard model is discovered at the LHC or other experiments, a_μ will constitute an indispensable tool to discriminate between very different types of new physics, especially since it is highly sensitive to parameters which are difficult to measure at the LHC. If no new phenomena are found elsewhere, then it represents one of the few ways to probe physics beyond the standard model. In either case, it will play an essential and complementary role in the quest to understand physics beyond the standard model at the TeV scale.

The muon magnetic moment has a special role because it is sensitive to a large class of models related and unrelated to electroweak symmetry breaking and because it combines several properties in a unique way: it is a flavor- and CP-conserving, chirality-flipping and loop-induced quantity. In contrast, many high-energy collider observables at the LHC and a future linear collider are chirality-conserving, and many other low-energy precision observables are CP- or flavor-violating. These unique properties might be the reason why the muon $(g-2)$ is the only among the mentioned observables which shows a significant deviation between the experimental value and the SM prediction. Furthermore, while $g-2$ is sensitive to leptonic couplings, b- or K-physics more naturally probe the hadronic couplings of new physics. If charged lepton-flavor violation exists, observables such as $\mu \to e$ conversion can only determine a combination of the strength of lepton-flavor violation and the mass scale of new physics. In that case, $g-2$ can help to disentangle the nature of the new physics.

(((I would like to reduce this entire thing below to one table. BCKC)))))

Unravelling the existence and the properties of such new physics requires experimental information complementary to the LHC. The muon $(g-2)$, together with searches for charged lepton flavor violation, electric dipole moments, and rare decays, belongs to a class of complementary low-energy experiments.

In fact, The role of $g-2$ as a discriminator between very different standard model extensions is well illustrated by a relation stressed by Czarnecki and Marciano [60]. It holds in a wide range of models as a result of the chirality-flipping nature of both $g-2$ and the muon mass: If a new physics model with a mass scale Λ contributes to the muon mass $\delta m_\mu(\text{N.P.})$, it also contributes to a_μ, and the two contributions are related as

$$a_\mu(\text{N.P.}) = \mathcal{O}(1) \times \left(\frac{m_\mu}{\Lambda}\right)^2 \times \left(\frac{\delta m_\mu(\text{N.P.})}{m_\mu}\right). \tag{1.15}$$

The ratio $C(\text{N.P.}) \equiv \delta m_\mu(\text{N.P.})/m_\mu$ cannot be larger than unity unless there is fine-tuning in the muon mass. Hence a first consequence of this relation is that new physics can explain the currently observed deviation (**??**) only if Λ is at the few-TeV scale or smaller.

In many models, the ratio C arises from one- or even two-loop diagrams, and is then suppressed by factors like $\alpha/4\pi$ or $(\alpha/4\pi)^2$. Hence, even for a given Λ, the contributions to a_μ are highly model dependent.

It is instructive to classify new physics models as follows:

- Models with $C(\text{N.P.}) \simeq 1$: Such models are of interest since the muon mass is essentially generated by radiative effects at some scale Λ. A variety of such models have been discussed in [60], including extended technicolor or generic models with naturally vanishing bare muon mass. For examples of radiative muon mass generation within supersymmetry, see e.g. [78, 79]. In these models the new physics contribution to a_μ can be very large,

$$a_\mu(\Lambda) \simeq \frac{m_\mu^2}{\Lambda^2} \simeq 1100 \times 10^{-11} \left(\frac{1\ \text{TeV}}{\Lambda}\right)^2 . \tag{1.16}$$

  and the difference Eq. (**??**) can be used to place a lower limit on the new physics mass scale, which is in the few TeV range [80, 79].

- Models with $C(\text{N.P.}) = \mathcal{O}(\alpha/4\pi)$: Such a loop suppression happens in many models with new weakly interacting particles like Z' or W', little Higgs or certain extra dimension models. As examples, the contributions to a_μ in a model with $\delta = 1$ (or 2) universal extra dimensions (UED) [81] and the Littlest Higgs model with T-parity (LHT) [82] are given by with $|S_{\text{KK}}| \lesssim 1$ [81]. A difference as large as Eq. (**??**) is very hard to accommodate unless the mass scale is very small, of the order of M_Z, which however is often excluded e.g. by LEP measurements. So typically these models predict very small contributions to a_μ and will be disfavored if the current deviation will be confirmed by the new a_μ measurement.

  Exceptions are provided by models where new particles interact with muons but are otherwise hidden from searches. An example is the model with a new gauge boson associated to a gauged lepton number $L_\mu - L_\tau$ [83], where a gauge boson mass of $\mathcal{O}(100\ \text{GeV})$ and large a_μ are viable.

- Models with intermediate values for $C(\text{N.P.})$ and mass scales around the weak scale: In such models, contributions to a_μ could be as large as Eq. (**??**) or even larger, or smaller, depending on the details of the model. This implies that a more precise a_μ-measurement will have significant impact on such models and can even be used to measure model parameters. Supersymmetric (SUSY) models are the best known examples, so muon $g-2$ would have substantial sensitivity to SUSY particles. Compared to generic perturbative models, supersymmetry provides an enhancement to $C(\text{SUSY}) = \mathcal{O}(\tan\beta \times \alpha/4\pi)$ and to $a_\mu(\text{SUSY})$ by a factor $\tan\beta$ (the ratio of the vacuum expectation values of the two Higgs fields). Typical SUSY diagrams for the magnetic dipole moment, the electric dipole moment, and the lepton-number violating conversion process $\mu \to e$ in the field of a nucleus are shown pictorially in Fig. **??**. The shown diagrams contain the SUSY partners of the muon, electron and the SM $\text{U}(1)_Y$ gauge boson, $\tilde{\mu}$, $\tilde{e}$, $\tilde{B}$. The full SUSY contributions involve also the SUSY partners to the neutrinos and all SM gauge and Higgs bosons. In a model with SUSY masses equal to Λ the SUSY contribution to a_μ is given by [60]

$$a_\mu(\text{SUSY}) \simeq \text{sgn}(\mu)\ 130 \times 10^{-11}\ \tan\beta\ \left(\frac{100\ \text{GeV}}{\Lambda}\right)^2 \tag{1.17}$$

  which indicates the dependence on $\tan\beta$, and the SUSY mass scale, as well as the sign of the SUSY μ-parameter. The formula still approximately applies even if only the smuon and chargino masses are of the order Λ but e.g. squarks and gluinos are much heavier. However the SUSY contributions to a_μ

depend strongly on the details of mass splittings between the weakly interacting SUSY particles. Thus muon $g-2$ is sensitive to SUSY models with SUSY masses in the few hundred GeV range, and it will help to measure SUSY parameters.

There are also non-supersymmetric models with similar enhancements. For instance, lepton flavor mixing can help. An example is provided in Ref. [84] by a model with two Higgs doublets and four generations, which can accommodate large Δa_μ without violating constraints on lepton flavor violation. In variants of Randall-Sundrum models [85, 86, 87] and large extra dimension models [88], large contributions to a_μ might be possible from exchange of Kaluza-Klein gravitons, but the theoretical evaluation is difficult because of cutoff dependences. A recent evaluation of the non-graviton contributions in Randall-Sundrum models, however, obtained a very small result [89].

Further examples include scenarios of unparticle physics [90, 91] (here a more precise a_μ-measurement would constrain the unparticle scale dimension and effective couplings), generic models with a hidden sector at the weak scale [92] or a model with the discrete flavor symmetry group T' and Higgs triplets [93] (here a more precise a_μ-measurement would constrain hidden sector/Higgs triplet masses and couplings), or the model proposed in Ref. [94], which implements the idea that neutrino masses, leptogenesis and the deviation in a_μ all originate from dark matter particles. In the latter model, new leptons and scalar particles are predicted, and a_μ provides significant constraints on the masses and Yukawa couplings of the new particles.

The following types of new physics scenarios are quite different from the ones above:

- Models with extended Higgs sector but without the $\tan\beta$-enhancement of SUSY models. Among these models are the usual two-Higgs-doublet models. The one-loop contribution of the extra Higgs states to a_μ is suppressed by two additional powers of the muon Yukawa coupling, corresponding to $a_\mu(\text{N.P.}) \propto m_\mu^4/\Lambda^4$ at the one-loop level. Two-loop effects from Barr-Zee diagrams can be larger [95], but typically the contributions to a_μ are negligible in these models.
- Models with additional light particles with masses below the GeV-scale, generically called dark sector models: Examples are provided by the models of Refs. [96, 97], where additional light neutral gauge bosons can affect electromagnetic interactions. Such models are intriguing since they completely decouple $g-2$ from the physics of EWSB, and since they are hidden from collider searches at LEP or LHC (see however Refs. [98, 99] for studies of possible effects at dedicated low-energy colliders and in Higgs decays at the LHC). They can lead to contributions to a_μ which are of the same order as the deviation in Eq. (**??**). Hence the new $g-2$ measurement will provide an important test of such models.

To summarize: many well-motivated models can accommodate larger contributions to a_μ — if any of these are realized $g-2$ can be used to constrain model parameters; many well-motivated new physics models give tiny contributions to a_μ and would be disfavored if the more precise $g-2$ measurement confirms the current deviation. There are also examples of models which lead to similar LHC signatures but which can be distinguished using $g-2$.

1.3.2 Muon $g-2$: Experiment

Measurements of the magnetic and electric dipole moments make use of the torque on a dipole in an external field, $\vec{\tau} = \vec{\mu} \times \vec{B} + \vec{d} \times \vec{E}$. All muon MDM experiments except the original Nevis ones used polarized muons in flight, and measured the rate at which the spin turns relative to the momentum, $\vec{\omega}_a = \vec{\omega}_S - \vec{\omega}_C$, when a

beam of polarized muons is injected into a magnetic field. The resulting frequency, assuming that $\vec{\beta} \cdot \vec{B} = 0$, is given by [69, 70]

$$\vec{\omega}_{a\eta} = \vec{\omega}_a + \vec{\omega}_\eta = -\frac{Qe}{m}\left[a\vec{B} + \left(a - \left(\frac{m}{p}\right)^2\right)\frac{\vec{\beta}\times\vec{E}}{c}\right] - \eta\frac{Qe}{2m}\left[\frac{\vec{E}}{c} + \vec{\beta}\times\vec{B}\right]. \tag{1.18}$$

Important features of this equation are the motional magnetic and electric fields: $\vec{\beta}\times\vec{E}$ and $\vec{\beta}\times\vec{B}$.

The E821 Collaboration working at the Brookhaven AGS used an electric quadrupole field to provide vertical focusing in the storage ring, and shimmed the magnetic field to 1 ppm uniformity on average. The storage ring was operated at the " $g-2$" momentum, $p_{g-2} = 3.094$ GeV/c, ($\gamma_{g-2} = 29.3$), so that $a_\mu = (m/p)^2$ and the electric field did not contribute to ω_a. They obtained[36]

$$a_\mu^{(\mathrm{E821})} = 116\,592\,089(63) \times 10^{-11} \quad (0.54\,\mathrm{ppm}) \tag{1.19}$$

The final uncertainty of 0.54 ppm consists of a 0.46 ppm statistical component and a 0.28 ppm systematic component.

The present limit on the EDM also comes from E821 [72]

$$d_\mu = (0.1 \pm 0.9) \times 10^{-19} e\cdot\mathrm{cm};\ |d_\mu| < 1.9 \times 10^{-19} e\cdot\mathrm{cm}\ (95\%\ \mathrm{C.L.})\,, \tag{1.20}$$

so the EDM contribution to the precession is very small. In the muon $g-2$ experiments, the motional electric field dominates the ω_η term, which means that $\vec{\omega}_a$ and $\vec{\omega}_\eta$ are orthogonal. The presence of an EDM in the $g-2$ momentum experiments has two effects: the measured frequency is the quadrature sum of the two frequencies, $\omega = \sqrt{\omega_a^2 + \omega_\eta^2}$, and the EDM causes a tipping of the plane of precession, by an angle $\delta = \tan^{-1}[\eta\beta/(2a_\mu)]$. This tipping results in in an up-down oscillation of the decay positrons relative to the midplane of the storage ring with frequency ω_a *out of phase by* $\pi/2$ with the a_μ precession.

The E989 collaboration at Fermilab will move the E821 muon storage ring to Fermilab, and will use the $g-2$ momentum technique to measure a_{μ^+}. New detectors and electronics, and a beam handling scheme that increases the stored muon rate per hour by a factor of 6 over E821 will be implemented. The goal is at least 21 times the statistics of E821, and a factor of four overall uncertainty reduction, with equal systematic and statistical uncertainties of ± 0.1 ppm.

The scope of Project X includes 50-200kW of beam power at 8 GeV, about three to fifteen times the beam power of E989. This large step in beam power could be used to measure $g-2$ for negative muons, and provide muon beams with lower emittance thereby reducing experimental systematics.

Given the high impact of the E821 result and the crucial role the value of $g-2$ plays in interpreting energy frontier results, it is imperative to have a second measurement with at least equal precision but with a complementary approach to the measurement. An alternate approach planned for J-PARC [73] uses a much lower muon energy, and does not use the $g-2$ momentum technique. A surface muon beam produced by the low energy Booster is brought to rest in an aerogel target, where muonium (the μ^+e^- atom) is formed. The muonium is ionized by a powerful laser which produces a very slow muon beam with extremely small emittance. This low emittance beam is then accelerated by a linac to 300 MeV, and injected into a ~ 1 m diameter solenoidal magnet with point to point uniformity of ± 1 ppm, approximately 100 times better than at the Brookhaven experiment. The average uniformity is expected to be known to better then 0.1 ppm. The decays are detected by a full volume tracker consisting of an array of silicon detectors. This provides time, energy, and decay angle information for every positron, maximizing the sensitivity to separate the $g-2$ and EDM precession frequencies. The expected $g-2$ sensitivity is comparable to the Fermilab experiment but will have very different systematic uncertainties and the combined results from the two experiments should bring the precision to below the 100 ppb level.

1.3.3 Muon $g-2$: Expected improvements in the Predicted Value

(((((This can be shortened, updated, and add a table that has the expected improvements)))))

The QED and e;ectroweak contributions to $g-2$ can be calculated to from first principles and and are regarded as robust. The two dominant QCD contributions are hadronic vacuum polarization(HPV) and hadronic light-by-light contribution (HLBL) The HVP contribution to a_μ can be determined from the cross-section for $e^+e^- \to$ hadrons (and over a certain energy range, by $\tau \to$ hadrons) and a dispersion relation. It can also be computed from purely first principles using lattice QCD to calculate the HVP directly [46]. The two methods are complementary and can be used to check each other. The current best uncertainty comes from the first method,

$$a_\mu(\text{HVP}) = (692.3 \pm 4.2) \times 10^{-10}, \tag{1.21}$$

or about 0.61% [41] when only e^+e^- data are used. If τ data are included, $a_\mu = 701.5 \pm 4.7 \times 10^{-10}$, or 0.67% (but see [45] for the analysis that brings the τ into good agreement with e^+e^-). In the next 3-5 years the uncertainty on a_μ(HVP) is expected to drop by roughly a factor of 2, relying on new results from *BABAR*, Belle, BES, and VEPP2000. The lattice calculations presently have an uncertainty of about 5% [47, 48, 49, 50], which is expected to decrease to 1-2% in the next 3-5 years [51]. At the one-percent level contributions from the charm and so-called disconnected diagrams (right panel, Fig. 1-9) enter. Both are currently under investigation.

The hadronic-light-by-light (HLbL) scattering amplitude shown in Fig. 1-10 is much more challenging. The contribution to $g-2$,

$$a_\mu(\text{HLbL}) = 105(26) \times 10^{-11}, \tag{1.22}$$

is not well known. It is based on the size of various hadronic contributions estimated in several different models [52]. Its uncertainty, though less than that in a_μ(HVP) by about a factor of two, seems harder to reduce and is expected to be the dominant uncertainty as the HVP uncertainty is reduced. Finding a new approach, such as lattice QCD, in which uncertainties are systematically improvable, is crucial for making greatest use of the next round of experiments. With this in mind, a workshop was recently convened at the Institute for Nuclear Theory [53]. Workshop participants discussed how models, lattice QCD, and data-driven methods could be exploited to reduce the uncertainty on a_μ(HLbL). The outcome of this workshop is that a SM calculation of the HLbL contribution with a total uncertainty of 10%, or less, can be achieved within five years. A detailed discussion of the computation of a_μ(HLbL) in lattice QCD is given in the USQCD Collaboration white paper on $g-2$ [51].

There are two methods, using the lattice framework, under investigation. The conventional one, analogous to the HVP calculation, is to calculate the correlation function of four electromagnetic currents for the quarks in pure QCD, one for each possible, independent, momentum configuration (there are V^2), fit the

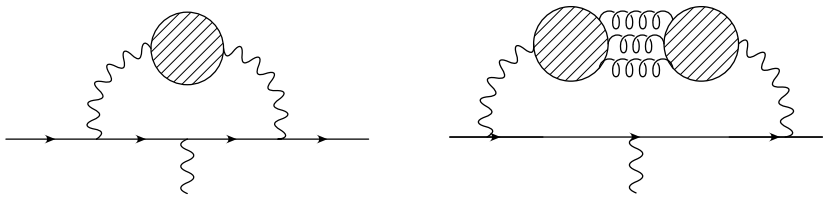

Figure 1-9. *Hadronic vacuum polarization diagrams contributing to the SM muon anomaly. The horizontal lines represent the muon. (Left panel) The blob formed by the quark-antiquark loop represents all possible hadronic intermediate states. (Right panel) Disconnected quark line contribution. The quark loops are connected by gluons.*

resulting function of discrete momenta to a smooth function and insert it into the two-loop QED integrals. The resulting four-Lorentz-index hadronic tensor has 32 independent contractions. For these reasons, the calculation is computationally demanding. An intermediate but useful step is to calculate the four-point correlation function at well chosen values of the vertex momenta to partially check model calculations.

A second method is to compute the entire amplitude on the lattice, including the muon, in a combined QED+QCD gauge field [54, 55, 56]. The method has passed several non-trivial tests. First, it has been successfully checked against perturbation theory in pure QED. Large finite volume effects (the photons are long range) appear manageable. Preliminary calculations in full QED+QCD, at unphysical quark and muon mass and momentum transfer q^2, show a statistically significant result. The method requires a non-perturbative subtraction of leading order in α contributions which has been checked by varying the strength of the electric charge in the calculations and observing the expected scaling, before and after the subtraction. Disconnected contributions like the one shown in the right panel of Fig. 1-10 have not been included yet, but will be once the simpler first diagram (left panel, same figure) is fully under control. Calculations on a larger volume with smaller masses are in progress.

In addition to these direct approaches, there is other ongoing work on lattice-QCD calculations that check or supplement the model calculations. For example, it is well-known that the pion pole (namely, $\gamma\gamma^* \to \pi^0 \to \gamma^*\gamma^*$) provides the largest contribution to the QCD blob in Fig. 1-10. Just as experiments are being mounted to examine this physics (*e.g.*, PrimEx at JLab and KLOE at LNF), several groups [57, 58, 59] are using lattice QCD to compute the amplitudes for $\pi^0 \to \gamma\gamma^*$ and $\pi^0 \to \gamma^*\gamma^*$ (with one or two virtual photons).

If the SM and experiment central values do not change while both experiment and theory uncertainties are reduced, the discrepancy between the two becomes irresistible. The improvement expected from E989 (0.14 PPM) by itself improves Δa_μ to 5σ. A simultaneous decrease in the HLbL uncertainty to 10% from the current 25% pushes it to 6σ, and finally, reducing the uncertainty on the HVP contribution by a factor of two increases it to 9 σ. Such a large and clear difference between experiment and the Standard Model for the muon $g-2$ will be extremely discriminating between new physics scenarios responsible for this discrepancy and will significantly leverage results from the energy frontier being explored at the LHC.

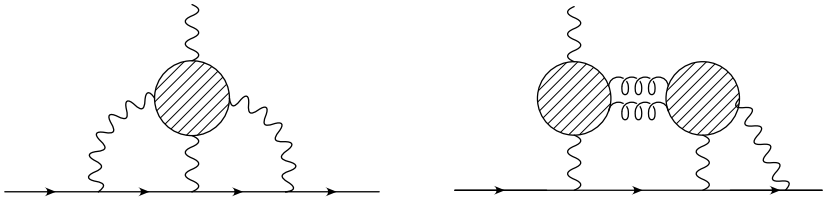

Figure 1-10. *Hadronic light-by-light scattering diagrams contributing to the SM muon anomaly. The horizontal lines represent the muon. (Left panel) The blob formed by the quark loop represents all possible hadronic intermediate states. (Right panel) One of the disconnected quark line contributions. The quark loops are connected by gluons.*

1.3.4 τ $g-2$ and EDM

1.3.5 Storage Ring EDMs

At the magic momentum, the equation for the spin procession frequency of a charged particle in a storage ring is given by

$$\vec{\omega}_{a\eta} = \vec{\omega}_a + \vec{\omega}_\eta = -a\frac{Qe}{m}\vec{B} - \eta\frac{Qe}{2m}\left[\frac{\vec{E}}{c} + \vec{\beta}\times\vec{B}\right]. \tag{1.23}$$

The precession frequency is by far dominated by the $a = (g-2)/2$ term. The key to extracting sensitivity to the EDM term η is to find ways of reducing or eliminating the motion due to the magnetic term a.

The first method is to use a magnetic storage ring such as the Muon g-2 experiment to extract a limit on the muon EDM. In the muon rest frame, the muon sees a strong motional electric field pointing towards the center of the ring adding a small horizontal component to the precession frequency vector that tilts the rotation plane. For a positive EDM, when the spin is pointing into the ring it will have a negative vertical component and when the spin is pointing to the outside of the ring it will have a positive vertical component. Since the positrons are emitted along the spin direction, this asymmetry maps into the positron decay angle. Since the asymmetry is maximized when the spin are perpendicular, the angular asymmetry is 90 degrees out of phase with the $g-2$ precession frequency. Searches for this asymmetry have been used to set limits on the muon EDM both at the CERN and Brookhaven $g-2$ experiments.

A number of the E989 detector stations will be instrumented with straw chambers to measure the decay positron tracks. With this instrumentation, a simultaneous EDM measurement can be made during the a_μ data collection, improving on the E821 muon EDM [72] limit by up to two orders of magnitude down to $\sim 10^{-21}\, e\cdot\text{cm}$. The J-PARC muon $g-2$ proposal also will have decay angle information for all tracks and expects a similar improvement.

To go beyond this level for the muon, will require a dedicated EDM experiment that uses the "frozen spin" method [74, 75]. The idea is to operate a muon storage ring off of the $g-2$ momentum and to use a radial electric field to cancel the ω_a term in Eq. 1.23, the $g-2$ precession. The electric field needed to freeze the spin is $E \simeq aBc\beta\gamma^2$. Once the spin is frozen, the EDM will cause a steadily increasing out-of-plane motion of the spin vector. One stores polarized muons in a ring with detectors above and below the storage region and forms the asymmetry (up - down)/(up + down). To reach a sensitivity of $10^{-24} e\cdot\text{cm}$ would require $\sim 4\times10^{16}$ recorded events [74]. Preliminary discussions have begun on a frozen spin experiment using the 1000 kW beam power available at the Project X 3 GeV rare process campus.

An alternative method is to remove the $g-2$ precession frequency completely by removing the magnet and using an electrostatic storage ring. This still requires the particle to be at the magic momentum to cancel the motional magnetic field. For these experiments, counter rotating beams are used to cancel the dominant systematic effects associated with stray magnetic fields. This idea has been studied in detail for the proton and deuteron with projected sensitivities approaching 10^{-30} using fairly large storage rings an proton momenta of 700 MeV.

For the electron, the magic momentum is 15 MeV. The smaller momentum would allow for a much smaller storage ring. Initial studies indicate that sensitivities up to 10^{-27} ·cm can be achieved which would be competitive with current limits and would be the best limits for a bare fermion. Furthermore, this would act as a much smaller test bed for the proton storage ring EDM experiment and would help demonstrate that the systematic uncertainties could be controlled.

(((((((Add a few paragraphs about the details of the electron proposal)))))))

1.3.6 Parity-Violating Experiments

Ultra-precise measurements of weak neutral current amplitudes in fixed target experiments provide a complementary indirect probe of new TeV-scale dynamics in flavor-conserving processes. In order to match the sensitivity of future collider searches and other indirect probes, it is necessary to measure amplitudes with an uncertainty approaching $10^{-3} \times G_F$. The technique of parity-violating electron scattering, in which one measures the fractional difference A_{PV} in the cross-section for longitudinally polarized electrons scattering from unpolarized targets, has attained the sensitivity to make important contributions to a comprehensive search for new TeV-scale dynamics in the flavor-conserving sector [128].

A comprehensive discussion of leptonic and semi-leptonic weak neutral current processes, their respective sensitivitiies, and complementarity are discussed in Sec. XX of the Working Group on Nuclei and Atoms. In the following, we focus on a particular purely-leptonic measurement, A_{PV} in electron-electron (Møller) scattering. The SLAC E158 experiment made the first measurement of this observable [130], and set important complementary limits on contact interactions with a sensitivity comparable to the highest energy colliders that were then running in parallel *i.e.*, LEP-II and the Tevatron.

The MOLLER experiment proposed at Jefferson Laboratory can improve on the E158 measurement by more than a factor of 5, taking advantage of the energy upgrade of the high intensity polarized electron beam to 11 GeV [129]. The goal is a measurement of A_{PV} to a fractional accuracy of 2.3%. The electron beam energy, luminosity and stability at Jefferson Laboratory are uniquely suited to carry out such a measurement. The compelling opportunity that this initiative represents can be summarized in three inter-related bullets:

1. The proposed A_{PV} measurement is sensitive to new neutral current interaction amplitudes as small as $1.5 \times 10^{-3} \cdot G_F$, which corresponds to a sensitivity of $\Lambda/g = 7.5$ TeV, where Λ/g, where g characterizes the strength and Λ is the scale of the new dynamics. .This would be *the* most sensitive probe of new flavor and *CP*-conserving neutral current interactions in the leptonic sector until the advent of new lepton collider or a neutrino factory.

2. The two most precise determinations of $\sin^2\theta_W$, carried out at the Z^0 pole, differ from each other by more than 3 standard deviations. While the world average is consistent with other electroweak measurements and the mass of the scalar resonance discovered at the LHC, choosing one or the other central value ruins this consistency and would imply very different kinds of new high-energy dynamics. The proposed A_{PV} measurement, which aims to achieve $\delta(\sin^2\theta_W) = \pm 0.00029$, may be able to resolve this discrepancy.

3. The proposed measurement would be carried out at $Q^2 \ll M_Z^2$, far from the Z^0. A convenient way to parametrize a class of new physics effects, to which Z^0 resonance observables are insensitive, is via the parameter $X(Q^2) \equiv \alpha^{-1}(\sin^2\theta_W(Q^2) - \sin^2\theta_W(M_Z^2)$. The projected MOLLER sensitivity is $\delta(X) \approx 0.035$. This is by far the most sensitive reach among similar potential measurements under discussion and probes a region of discovery space of new low energy flavor-conserving effective amplitudes that might be induced, for example, by dark photons with a tiny admixture of the Standard Model Z^0 boson [131].

A_{PV} in Møller scattering measures the weak charge of the electron Q_W^e, which is proportional to the product of the electron's vector and axial-vector couplings to the Z^0 boson. The electroweak theory prediction at tree

level in terms of the weak mixing angle is $Q_W^e = 1-4\sin^2\theta_W$; this is modified at the 1-loop level [132, 133, 134] and becomes dependent on the energy scale at which the measurement is carried out, *i.e.* $\sin^2\theta_W$ "runs". At low energy, Q_W^e is predicted to be 0.0469 ± 0.0006, a $\sim 40\%$ change of its tree level value of ~ 0.075 (when evaluated at M_Z).

The value of A_{PV} at the MOLLER energy is ≈ 35 parts per billion (ppb); the expected statistical precision is 0.73 ppb, providing a 2.3% measurement of Q_W^e. The reduction in the numerical value of Q_W^e due to radiative corrections leads to increased fractional accuracy in the determination of the weak mixing angle, $\sim 0.1\%$, comparable to the two best such determinations from measurements of asymmetries in Z^0 decays at LEP and SLC.

Figure. 1-11 shows the four best measurements from studies of Z^0 decays [135] as well as the projected uncertainty of the MOLLER proposal. Also shown is the Standard Model prediction for a Higgs mass (m_H) of 126 GeV. The grand average of the four measurements is consistent with the theoretical expectation, but the scatter in the measurements somewhat large; MOLLER would provide an additional measurement with comparable precision.

An additional important feature of the proposed measurement is that it will be carried out at $Q^2 \ll M_Z^2$. The two best measurements of the weak mixing angle at lower energies are those extracted from the E158 [130], and the measurement of the weak charge of ^{133}Cs [136] via studies of atomic parity violation. The interpretation of the latter measurement in terms of an extraction of the weak mixing angle has been recently updated [137]. Figure 1-12 shows the dependence of $\sin^2\theta_W$ to m_H and the two best high energy and low energy measurements discussed above. Also shown is the projected error for the MOLLER proposal. Remarkably, many different versions of new dynamics at the TeV scale can have a significant impact on low Q^2 measurements while having little impact on Z^0 decay measurements, because interference effects on resonance are suppressed. There is still plenty of room for new physics effects to be discovered at low energy with the proposed A_{PV} uncertainty.

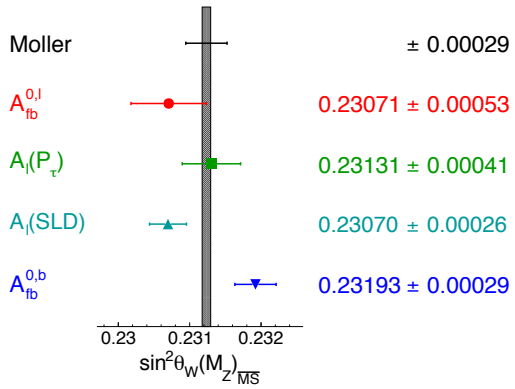

Figure 1-11. *The four best* $\sin^2\theta_W$ *measurements and the projected error of the MOLLER proposal. The black band represents the theoretical prediction for* $m_H = 126$ *GeV.*

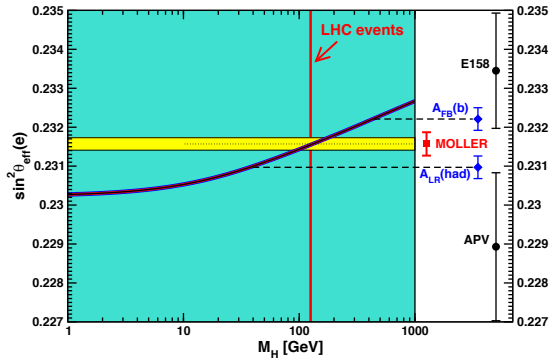

Figure 1-12. $\sin^2\theta_W$ *vs* m_H. *The yellow band shows the world average. The blue data points represent the two best high energy determinations while the black points are the most precise low energy determinations. The projected MOLLER error is shown in red.*

At the level of sensitivity probed, the proposed measurement could be influenced by radiative loop effects of new particles predicted by the Minimal Supersymmetric Standard Model (MSSM). The impact on the

weak charges of the electron and the proton $Q_W^{e,p}$ have been analyzed in detail [138]. A combined analysis of precision low energy measurements of both charged and neutral current processes can be found in a comprehensive review [139], which has been recently updated [140]. Inspecting a random scan over a set of MSSM parameters whose values are consistent with current precision measurements as well as the most recent LHC search limits from 7 and 8 TeV running, A_{PV} would see in the effects in the range of 2 and 3 σ at larger values of the MSSM parameter $\tan\beta$ (the ratio of vacuum expectation values of the model's two Higgs scalars) or if one of the superpartner masses is relatively light. If the assumption of R-parity conservation is relaxed (RPV), tree-level interactions could generate deviations in A_{PV} of opposite sign and similar magnitude. Thus, if nature is supersymmetric, the proposed measurement would shed light on an important followup question regarding the validity of R-parity symmetry.

A comprehensive analysis of the MOLLER sensitivity to TeV-scale Z's has been carried out [141] for a class of family-universal models contained in the E_6 gauge group. While models with full E_6 unification are already excluded by existing precision electroweak data, the Z' bosons in these models with the same electroweak charges to SM particles are still motivated, since they also arise in many superstring models as well as from a bottom-up approach [142]. A_{PV} probes $M_{Z'}$ of order 2.5 TeV, comparable to the anticipated reach of early LHC running after the energy ramp-up to 13 TeV. The reach of A_{PV} would be further enhanced in comparison to direct searches if one relaxes the model-dependent assumption of GUT coupling strength; indirect deviations scale linearly with other values of the coupling strength whereas dilepton production at colliders has a much milder dependence on this parameter.

The measurement would be carried out in Hall A at Jefferson Laboratory, where a 11 GeV longitudinally polarized electron beam would be incident on a 1.5 m liquid hydrogen target. Møller electrons (beam electrons scattering off target electrons) in the full range of the azimuth and spanning the polar angular range 5 mrad $< \theta_{lab} <$ 17 mrad, would be separated from background and brought to a ring focus $\sim$ 30 m downstream of the target by a spectrometer system consisting of a pair of toroidal magnet assemblies and precision collimators. The Møller ring would be intercepted by a system of quartz detectors; the resulting Cherenkov light would provide a relative measure of the scattered flux. The experimental techniques for producing an ultra-stable polarized electron beam, systematic control at the part per billion level, calibration techniques to control normalization errors including the degree of electron beam polarization at the 1% level have been continuously improved over fifteen years of development at JLab.

The 2012 NSAC subpanel on the implementation of the Long Range Panel (the Tribble Subcommittee) strongly endorsed the MOLLER project as part of the suite of investments advocated for the subfield of Fundamental Symmetries. JLab submitted a Major Item of Equipment (MIE) proposal to DoE on behalf of the MOLLER collaboration ($\sim$ 100 physicists from 30 institutions). The goal is to obtain construction funding by 2015, with the hope of installing the apparatus and commissioning the experiment in 2017/18.

1.4 Summary

References

[1] J. L. Hewett, H. Weerts, R. Brock, J. N. Butler, B. C. K. Casey, J. Collar, A. de Govea and R. Essig *et al.*, arXiv:1205.2671.

[2] R.J. Abrams et al. (Mu2e Collaboration and Project), *Mu2e Conceptual Design Report*, arXiv:1211.7019.

[3] W. H. Bertl, *et al.* (SINDRUM-II Collaboration), *Eur.Phys.J.* **C47**, 337–346 (2006).

[4] W.J. Marciano, T. Mori, and J.M. Roney, *Ann.Rev.Nucl.Part.Sci.*, 58:315–341, 2008.

[5] A. de Gouvea and P. Vogel, arXiv:1303.4097.

[6] A. Czarnecki, X. Garcia i Tormo, W.J. Marciano, Phys. Rev. D **84**, 013006 (2011).

[7] K. Knoepfel et al. , *Mu2e-II White Paper*, arXiv:1307.????.

[8] A. Kronfeld et al. , *Project X: Physics Opportunities*, arXiv:1307.????.

[9] R. Kitano, M. Koike and Y. Okada, Phys. Rev. D **66**, 096002 (2002) [Erratum-ibid. D **76**, 059902 (2007)].

[10] V. Cirigliano, R. Kitano, Y. Okada and P. Tuzon, Phys. Rev. D **80**, 013002 (2009).

[11] For more information see http://www.muonsinc.com/muons3/G4beamline.

[12] M. Asai, Geant4– a simulation toolkit. *Trans. Amer. Nucl. Soc.*, 95:757, 2006.

[13] Bob Tshirhart, private communication, April 2013.

[14] T. Suzuki, D. F. Measday and J. P. Roalsvig, Phys. Rev. C **35**, 2212 (1987).

[15] We investigated the possibility of also beginning the live gate at an earlier time, but this resulted in an unacceptable increase in background events from radiative pion captures.

[16] Note that the DIO estimate for the titanium stopping target is an extrapolation from a detailed simulation of the aluminum DIO spectrum scaled to obtain the correct endpoint for titanium. Work is underway to include the titanium DIO spectrum in the simulation software and repeat this estimate.

[17] R.J. Abrams et al. Mu2e Conceptual Design Report. 2012.

[18] J. Adam et al. New constraint on the existence of the $\mu^+ \to e^+\gamma$ decay. *Phys. Rev. Lett.*, 110:201801, 2013.

[19] A.M. Baldini, F. Cei, C. Cerri, S. Dussoni, L. Galli, et al. MEG Upgrade Proposal. 2013.

[20] A. Blondel, A. Bravar, M. Pohl, S. Bachmann, N. Berger, et al. Research Proposal for an Experiment to Search for the Decay $\mu \to eee$. 2013.

[21] Adriana Bungau, Robert Cywinski, Cristian Bungau, Philip King, and James Lord. Simulations of surface muon production in graphite targets. *Phys.Rev.ST Accel.Beams*, 16:014701, 2013.

[22] G. Heidenreich. Carbon and Beryllium Targets at PSI. *AIP Conf.Proc.*, 642:122–124, 2003.

[23] A. Hillairet et al. Precision muon decay measurements and improved constraints on the weak interaction. *Phys. Rev. D*, 85:092013, 2012.

[24] A.E. Pifer, T. Bowen, and K.R. Kendall. A High Stopping Density mu+ Beam. *Nucl.Instrum.Meth.*, 135:39–46, 1976.

[25] S. Striganov. Low energy muon production estimates at Project X, 2012. https://indico.fnal.gov/getFile.py/access?contribId=21&sessionId=4&resId=0&materialId=slides&confId=6025.

[26] V. Tishchenko et al. Detailed Report of the MuLan Measurement of the Positive Muon Lifetime and Determination of the Fermi Constant. *Phys. Rev. D*, 87:052003, 2013.

[27] O.B. Van Dyck, E.W. Hoffman, R.J. Macek, G. Sanders, R.D. Werbeck, et al. 'Cloud' and 'Surface' Muon Beam Characteristics. *IEEE Trans.Nucl.Sci.*, 26:3197–3199, 1979.

[28] J. Adam *et al.* [MEG Collaboration], arXiv:1303.0754 [hep-ex].

[29] F. Dejongh, Presentation at the 2012 Project X Summer Study, https://indico.fnal.gov/getFile.py/access?contribId=77&sessionId=10&resId=0&materialId=slides&confId=5276.

[30] A. M. Baldini, F. Cei, C. Cerri, S. Dussoni, L. Galli, M. Grassi, D. Nicolo and F. Raffaelli *et al.*, arXiv:1301.7225 [physics.ins-det].

[31] P.A.M. Dirac, Proc. R. Soc. (London) **A117**, 610 (1928).

[32] J. Schwinger, Phys. Rev. **73**, 416L (1948), and Phys. Rev. **76** 790 (1949). The former paper contains a misprint in the expression for a_e that is corrected in the longer paper.

[33] R.L. Garwin, L.M. Lederman, M. Weinrich, Phys. Rev. **105**, 1415, (1957).

[34] R.L. Garwin, D.P. Hutchinson, S. Penman and G. Shapiro, Phys. Rev. **118**, 271 (1960).

[35] G. Charpak *et al.*, Phys. Rev. Lett. **6**, 128 (1961), Nuovo Cimento **22**, 1043 (1961), Phys. Lett. **1**, 16 (1962), and Nuovo Cimento **37** 1241 (1965), G. Charpak, et al, Phys. Lett. **1**, 16 (1962).

[36] G. Bennett, *et al.*, (Muon $(g-2)$ Collaboration), Phys. Rev. **D73**, 072003 (2006).

[37] E.M. Purcell and N.F. Ramsey, Phys. Rev. **78**, 807 (1950).

[38] L. Landau, Nucl. Phys. **3**, 127 (1957).

[39] N.F. Ramsey Phys. Rev. **109**, 225 (1958).

[40] G. W. Bennett *et al.* [Muon G-2 Collaboration], Phys. Rev. D **73**, 072003 (2006) [hep-ex/0602035].

[41] M. Davier, A. Hoecker, B. Malaescu and Z. Zhang, Eur. Phys. J. C **71**, 1515 (2011) [arXiv:1010.4180 [hep-ph]].

[42] T. Teubner, K. Hagiwara, R. Liao, A. D. Martin and D. Nomura, Nucl. Phys. Proc. Suppl. **218**, 225 (2011).

[43] T. Aoyama, M. Hayakawa, T. Kinoshita and M. Nio, arXiv:1110.2826 [hep-ph].

[44] A. Czarnecki, W. J. Marciano and A. Vainshtein, Phys. Rev. D **67**, 073006 (2003) [Erratum-ibid. D **73**, 119901 (2006)] [hep-ph/0212229].

[45] F. Jegerlehner and R. Szafron, Eur. Phys. J. C **71**, 1632 (2011) [arXiv:1101.2872 [hep-ph]].

[46] T. Blum, Phys. Rev. Lett. **91**, 052001 (2003) [hep-lat/0212018].

[47] C. Aubin and T. Blum, Phys. Rev. D **75**, 114502 (2007) [hep-lat/0608011].

[48] X. Feng, K. Jansen, M. Petschlies and D. B. Renner, Phys. Rev. Lett. **107**, 081802 (2011) arXiv:1103.4818 [hep-lat].

[49] P. Boyle, L. Del Debbio, E. Kerrane and J. Zanotti, arXiv:1107.1497 [hep-lat].

[50] M. Della Morte, B. Jager, A. Juttner and H. Wittig, arXiv:1112.2894 [hep-lat].

[51] `http://www.usqcd.org/collaboration.html`

[52] J. Prades, E. de Rafael and A. Vainshtein, (Advanced series on directions in high energy physics. 20) [arXiv:0901.0306 [hep-ph]].

[53] Institute for Nuclear Theory Workshop, "Hadronic Light by Light Contribution to the muon g-2", February 28-March 4, 2011, Seattle, `http://www.int.washington.edu/PROGRAMS/11-47w/`

[54] A. Duncan, E. Eichten and H. Thacker, Phys. Rev. Lett. **76**, 3894 (1996) [hep-lat/9602005].

[55] M. Hayakawa, T. Blum, T. Izubuchi and N. Yamada, PoSLAT **2005**, 353 (2006) [hep-lat/0509016].

[56] T. Blum and S. Chowdhury, Nucl. Phys. Proc. Suppl. **189**, 251 (2009).

[57] S. D. Cohen, H. -W. Lin, J. Dudek and R. G. Edwards, PoSLATTICE **2008**, 159 (2008) [arXiv:0810.5550 [hep-lat]].

[58] E. Shintani *et al.* [JLQCD Collaboration], PoSLAT **2009**, 246 (2009) [arXiv:0912.0253 [hep-lat]].

[59] X. Feng et al., PoS Lattice2011 (2011)

[60] Andrzej Czarnecki and William J. Marciano, Phys. Rev. **D64** 013014 (2001).

[61] M. Blanke, A. J. Buras, B. Duling, A. Poschenrieder and C. Tarantino, JHEP **0705** (2007) 013 [arXiv:hep-ph/0702136].

[62] T. Appelquist and B. A. Dobrescu, "Universal extra dimensions and the muon magnetic moment," Phys. Lett. B **516** (2001) 85 [arXiv:hep-ph/0106140].

[63] D. Stöckinger, J. Phys. G G **34** (2007) R45.

[64] D. W. Hertzog, J. P. Miller, E. de Rafael, B. Lee Roberts and D. Stöckinger, arXiv:0705.4617 [hep-ph].

[65] M. Alexander, S. Kreiss, R. Lafaye, T. Plehn, M. Rauch, and D. Zerwas, Chapter 9 in M. M. Nojiri *et al.*, arXiv:0802.3672 [hep-ph].

[66] C. Adam, J. -L. Kneur, R. Lafaye, T. Plehn, M. Rauch and D. Zerwas, Eur. Phys. J. C **71** (2011) 1520 [arXiv:1007.2190 [hep-ph]].

[67] P. Bechtle, B. Sarrazin, K. Desch, H. K. Dreiner, P. Wienemann, M. Kramer, C. Robens and B. O'Leary, Phys. Rev. D **84** (2011) 011701 [arXiv:1102.4693 [hep-ph]].

[68] O. Buchmueller, R. Cavanaugh, A. De Roeck, M. J. Dolan, J. R. Ellis, H. Flacher, S. Heinemeyer and G. Isidori *et al.*, arXiv:1110.3568 [hep-ph].

[69] L.H. Thomas, Nature **117**, (1926) 514 and Phil. Mag. **3** (1927) 1.

[70] V. Bargmann, L. Michel, and V. L. Telegdi, Phys. Rev. Lett. **2**, 435 (1959).

[71] M. Davier, et al., Eur. Phys. J. **C 71**, 1515 (2011).

[72] G.W. Bennett, et al. (Muon G-2 Collaboration), Phys. Rev. **D 80**, 052008 (2009).

[73] Mibe, T, *Nucl. Phys. B (Proc. Suppl.)* 218:242 (2011)

[74] F.J.M. Farley et al., Phys. Rev. Lett. **93**, 052001 (2004)

[75] B. Lee Roberts, James P. Miller and Yannis K. Semertzidis, in *Lepton Dipole Moments*, B. Lee Roberts and William J. Marciano, ed., Advanced Series on Directions in High Energy Physics, V 20, World Scientific, 2010, p. 655.

[76] D. W. Hertzog, J. P. Miller, E. de Rafael, B. Lee Roberts and D. Stöckinger, arXiv:0705.4617 [hep-ph].

[77] The articles listed in the SPIRES citations to Ref. [**?**] contain many different models beyond the standard model.

[78] F. Borzumati, G. R. Farrar, N. Polonsky and S. D. Thomas, Nucl. Phys. B **555** (1999) 53 [hep-ph/9902443].

[79] A. Crivellin, J. Girrbach and U. Nierste, Phys. Rev. D **83** (2011) 055009 [arXiv:1010.4485 [hep-ph]].

[80] E. Eichten, et al., Phys. Rev. Lett. **45**, 225 (1980); K. Lane, arXiv [hep-ph/0102131].

[81] T. Appelquist and B. A. Dobrescu, Phys. Lett. B **516** (2001) 85 [arXiv:hep-ph/0106140].

[82] M. Blanke, A. J. Buras, B. Duling, A. Poschenrieder and C. Tarantino, JHEP **0705** (2007) 013 [arXiv:hep-ph/0702136].

[83] S. Baek, N. G. Deshpande, X. G. He and P. Ko, Phys. Rev. D **64**, 055006 (2001) [hep-ph/0104141]; E. Ma, D. P. Roy and S. Roy, Phys. Lett. B **525** (2002) 101 [hep-ph/0110146]; J. Heeck and W. Rodejohann, Phys. Rev. D **84** (2011) 075007 [arXiv:1107.5238 [hep-ph]].

[84] S. Bar-Shalom, S. Nandi and A. Soni, Phys. Lett. B **709**, 207 (2012) [arXiv:1112.3661 [hep-ph]].

[85] H. Davoudiasl, J. L. Hewett and T. G. Rizzo, Phys. Lett. B **493** (2000) 135 [arXiv:hep-ph/0006097].

[86] S. C. Park and H. S. Song, Phys. Lett. B **506** (2001) 99 [arXiv:hep-ph/0103072].

[87] C. S. Kim, J. D. Kim and J. H. Song, Phys. Lett. B **511** (2001) 251 [arXiv:hep-ph/0103127].

[88] M. L. Graesser, Phys. Rev. D **61** (2000) 074019 [arXiv:hep-ph/9902310].

[89] M. Beneke, P. Dey and J. Rohrwild, arXiv:1209.5897 [hep-ph].

[90] K. Cheung, W. Y. Keung and T. C. Yuan, Phys. Rev. Lett. **99** (2007) 051803 [arXiv:0704.2588 [hep-ph]].

[91] J. A. Conley and J. S. Gainer, arXiv:0811.4168 [hep-ph].

[92] D. McKeen, arXiv:0912.1076 [hep-ph].

[93] C. M. Ho and T. W. Kephart, Phys. Lett. B **687**, 201 (2010) [arXiv:1001.3696 [hep-ph]].

[94] T. Hambye, K. Kannike, E. Ma and M. Raidal, Phys. Rev. D **75** (2007) 095003 [arXiv:hep-ph/0609228].

[95] M. Krawczyk, Acta Phys. Polon. B **33**, 2621 (2002) [hep-ph/0208076].

[96] M. Pospelov, Phys. Rev. D **80** (2009) 095002 [arXiv:0811.1030 [hep-ph]].

[97] H. Davoudiasl, H. -S. Lee and W. J. Marciano, Phys. Rev. Lett. **109**, 031802 (2012) [arXiv:1205.2709 [hep-ph]].

[98] R. Essig, P. Schuster and N. Toro, Phys. Rev. D **80** (2009) 015003 [arXiv:0903.3941 [hep-ph]].

[99] H. Davoudiasl, H. -S. Lee and W. J. Marciano, Phys. Rev. D **86**, 095009 (2012) [arXiv:1208.2973 [hep-ph]].

[100] T. Moroi, Phys. Rev. D **53** (1996) 6565 [Erratum-ibid. **56** (1997) 4424].

[101] D. Stöckinger, J. Phys. G **34** (2007) R45 [arXiv:hep-ph/0609168].

[102] S. Heinemeyer, D. Stöckinger and G. Weiglein, Nucl. Phys. B **690** (2004) 62 [arXiv:hep-ph/0312264]; S. Heinemeyer, D. Stöckinger and G. Weiglein, Nucl. Phys. B **699** (2004) 103 [arXiv:hep-ph/0405255].

[103] A. Arhrib and S. Baek, Phys. Rev. D **65**, 075002 (2002) [hep-ph/0104225].

[104] R. Benbrik, M. Gomez Bock, S. Heinemeyer, O. Stal, G. Weiglein and L. Zeune, Eur. Phys. J. C **72**, 2171 (2012) [arXiv:1207.1096 [hep-ph]].

[105] A. Arbey, M. Battaglia, A. Djouadi and F. Mahmoudi, JHEP **1209**, 107 (2012) [arXiv:1207.1348 [hep-ph]].

[106] R. Ruiz de Austri, R. Trotta and L. Roszkowski, JHEP **0605** (2006) 002 [arXiv:hep-ph/0602028]; JHEP **0704** (2007) 084 [arXiv:hep-ph/0611173]; JHEP **0707** (2007) 075 [arXiv:0705.2012]; B. C. Allanach, C. G. Lester and A. M. Weber, JHEP **0612** (2006) 065; B. C. Allanach, K. Cranmer, C. G. Lester and A. M. Weber, JHEP **0708**, 023 (2007); J. R. Ellis, S. Heinemeyer, K. A. Olive, A. M. Weber and G. Weiglein, JHEP **0708** (2007) 083; S. Heinemeyer, X. Miao, S. Su and G. Weiglein, JHEP **0808**, 087 (2008).

[107] P. Bechtle, T. Bringmann, K. Desch, H. Dreiner, M. Hamer, C. Hensel, M. Kramer and N. Nguyen *et al.*, JHEP **1206**, 098 (2012) [arXiv:1204.4199 [hep-ph]].

[108] C. Balazs, A. Buckley, D. Carter, B. Farmer and M. White, arXiv:1205.1568 [hep-ph].

[109] O. Buchmueller, R. Cavanaugh, M. Citron, A. De Roeck, M. J. Dolan, J. R. Ellis, H. Flacher and S. Heinemeyer *et al.*, Eur. Phys. J. C **72**, 2243 (2012) [arXiv:1207.7315 [hep-ph]].

[110] M. Endo, K. Hamaguchi, S. Iwamoto, K. Nakayama and N. Yokozaki, Phys. Rev. D **85** (2012) 095006 [arXiv:1112.6412 [hep-ph]].

[111] M. Endo, K. Hamaguchi, S. Iwamoto and T. Yoshinaga, arXiv:1303.4256 [hep-ph].

[112] M. Ibe, T. T. Yanagida and N. Yokozaki, arXiv:1303.6995 [hep-ph].

[113] H. Baer, V. Barger, P. Huang and X. Tata, JHEP **1205** (2012) 109 [arXiv:1203.5539 [hep-ph]].

[114] M. Papucci, J. T. Ruderman and A. Weiler, JHEP **1209**, 035 (2012) [arXiv:1110.6926 [hep-ph]].

[115] T. J. LeCompte and S. P. Martin, Phys. Rev. D **85**, 035023 (2012) [arXiv:1111.6897 [hep-ph]].

[116] H. Murayama, Y. Nomura, S. Shirai and K. Tobioka, Phys. Rev. D **86**, 115014 (2012) [arXiv:1206.4993 [hep-ph]].

[117] B. A. Dobrescu and P. J. Fox, Eur. Phys. J. C **70** (2010) 263 [arXiv:1001.3147 [hep-ph]].

[118] W. Altmannshofer and D. M. Straub, JHEP **1009** (2010) 078 [arXiv:1004.1993 [hep-ph]].

[119] T. Appelquist, H. -C. Cheng and B. A. Dobrescu, Phys. Rev. D **64**, 035002 (2001) [hep-ph/0012100].

[120] I. Low, JHEP **0410**, 067 (2004) [hep-ph/0409025].

[121] J. Hubisz and P. Meade, Phys. Rev. D **71**, 035016 (2005) [hep-ph/0411264].

[122] J. M. Smillie and B. R. Webber, JHEP **0510** (2005) 069 [arXiv:hep-ph/0507170].

[123] Adam C, Kneur J -L, Lafaye R, Plehn T, Rauch M, Zerwas D. *Eur. Phys. J. C* 71:1520 (2011) [arXiv:1007.2190 [hep-ph]]

[124] N. Arkani-Hamed, G. L. Kane, J. Thaler and L. T. Wang, JHEP **0608**, 070 (2006) [arXiv:hep-ph/0512190].

[125] M. Alexander, S. Kreiss, R. Lafaye, T. Plehn, M. Rauch, and D. Zerwas, Chapter 9 in M. M. Nojiri *et al.*, *Physics Beyond the Standard Model: Supersymmetry,* arXiv:0802.3672 [hep-ph].

[126] B. C. Allanach *et al.*, *Proc. of the APS/DPF/DPB Summer Study on the Future of Particle Physics (Snowmass 2001)* ed. N. Graf, Eur. Phys. J. C **25** (2002) 113 [eConf **C010630** (2001) P125].

[127] C. F. Berger, J. S. Gainer, J. L. Hewett and T. G. Rizzo, JHEP **0902**, 023 (2009) [arXiv:0812.0980 [hep-ph]].

[128] K. S. Kumar, S. Mantry, W. J. Marciano and P. A. Souder, arXiv:1302.6263 [hep-ex].

[129] J. Dudek, R. Ent, R. Essig, K. S. Kumar, C. Meyer, R. D. McKeown, Z. E. Meziani and G. A. Miller *et al.*, Eur. Phys. J. A **48**, 187 (2012) [arXiv:1208.1244 [hep-ex]].

[130] P. L. Anthony *et al.* [SLAC E158 Collaboration], Phys. Rev. Lett. **95**, 081601 (2005) [hep-ex/0504049].

[131] H. Davoudiasl, H. -S. Lee and W. J. Marciano, Phys. Rev. Lett. **109**, 031802 (2012) [arXiv:1205.2709 [hep-ph]].

[132] A. Czarnecki and W. J. Marciano, Phys. Rev. D **53**, 1066 (1996) [hep-ph/9507420].

[133] A. Czarnecki and W. J. Marciano, Int. J. Mod. Phys. A **15**, 2365 (2000) [hep-ph/0003049].

[134] J. Erler and M. J. Ramsey-Musolf, Phys. Rev. D **72**, 073003 (2005) [hep-ph/0409169].

[135] [ALEPH and CDF and D0 and DELPHI and L3 and OPAL and SLD and LEP Electroweak Working Group and Tevatron Electroweak Working Group and SLD Electroweak and Heavy Flavour Groups Collaborations], arXiv:1012.2367 [hep-ex].

[136] S. C. Bennett and C. E. Wieman, Phys. Rev. Lett. **82**, 2484 (1999) [Erratum-ibid. **83**, 889 (1999)] [hep-ex/9903022].

[137] V. A. Dzuba, J. C. Berengut, V. V. Flambaum and B. Roberts, Phys. Rev. Lett. **109**, 203003 (2012) [arXiv:1207.5864 [hep-ph]].

[138] A. Kurylov, M. J. Ramsey-Musolf and S. Su, Phys. Rev. D **68**, 035008 (2003) [hep-ph/0303026].

[139] M. J. Ramsey-Musolf and S. Su, Phys. Rept. **456**, 1 (2008) [hep-ph/0612057].

[140] J. Erler and S. Su, Prog. Part. Nucl. Phys. **71**, 119 (2013) [arXiv:1303.5522 [hep-ph]].

[141] J. Erler, P. Langacker, S. Munir and E. Rojas, arXiv:1108.0685 [hep-ph].

[142] J. Erler, Nucl. Phys. B **586**, 73 (2000) [hep-ph/0006051].